Reactive scattering of oxygen and chlorine atoms on hydrocarbon surfaces
by Donna Joan Garton

A thesis submitted in partial fulfillment of the requirements for the degree of Master of Science in Chemistry
Montana State University

Abstract:
Reactions of free radicals, such as atomic oxygen and chlorine, with gaseous saturated hydrocarbons have been studied extensively due to their importance in combustion and atmospheric chemistry, respectively. Such reactions of the ground state species are known to proceed through direct hydrogen abstraction mechanisms. The detailed dynamical information of these reactions in the gas phase, especially with chlorine, make them ideal systems to study in analogous reactions of these free radicals with hydrocarbon surfaces. The study of atomic oxygen with hydrocarbon surfaces has been pursued by the space community, as naturally occurring atomic oxygen in low Earth orbit readily reacts with and degrades polymer materials on the outer surfaces of spacecraft; however, the detailed dynamics of the interaction has remained elusive. The atomic chlorine reactions are ideal comparative systems because of the wealth of gas phase data available. In this thesis, reactions of atomic oxygen, ground and electronically excited, and atomic chlorine with a liquid hydrocarbon surface have been investigated with a crossed molecular beams apparatus in order to understand the initial interactions occurring at the surface. Additional experiments to study the steady-state interactions of atomic oxygen with a solid hydrocarbon surface were also investigated.

In Chapter 4, interactions of ground and electronically excited atomic oxygen with a continuously refreshed film of a long-chain saturated hydrocarbon, squalane (C30H62), are discussed. Angularly-resolved flux and energy distributions of reactively-scattered products revealed that the dominant volatile reaction product is the OH radical, which can be formed by an Eley-Rideal direct-abstraction mechanism, similar to the gas-phase reaction, or by a process that leads to trapping and desorption of the initial product. Both these processes occur with comparable probabilities. A second, surface-unique product, H2O, is thought to be formed by abstraction of a hydrogen atom from the hydrocarbon chain by the primary OH product. The H2O product also exits the surface through nonthermal and thermal mechanisms, although the thermal mechanism dominates. The O(1D) does not react to form a volatile reaction product and is believed to insert into the hydrocarbon chain, as observed in gas phase reactions. Steady-state reactions of atomic oxygen with a hydrocarbon surface result in the formation of volatile CO and CO2, the end products of combustion, through thermal and nonthermal mechanisms.

A comparison of the dynamics of Cl(2P) and O(3P) reactions with a squalane surface is presented in Chapter 5. The only observable reaction product for the Cl reaction, HCl, was formed through two channels: 1) an Eley-Rideal direct abstraction mechanism, similar to observed Cl(2P) gas phase reactions and O(3P) reactions, and 2) thermal mechanism(s) not observed with oxygen. Construction of surface Newton Diagrams for the HCl and OH products allowed more specific comparison to gas-phase studies and a novel view of the role of the surface in these reactions.

Reactive Scattering of Oxygen and Chlorine Atoms on Hydrocarbon Surfaces

by

Donna Joan Garton

A thesis submitted in partial fulfillment
of the requirements for the degree

of

Master of Science

in

Chemistry

MONTANA STATE UNIVERSITY-BOZEMAN
Bozeman, Montana

July 1998

APPROVAL

of a thesis submitted by

Donna Joan Garton

This thesis has been read by each member of the thesis committee and has been found to be satisfactory regarding content, English usage, format, citations, bibliographic style, and consistency, and is ready for submission to the College of Graduate Studies.

Patrik R. Callis — Patrik R Callis — 25 Aug 98
Date

Approved for the Department of Chemistry

David M. Dooley — David M Dooley — Aug 25, 1998
Date

Approved for the College of Graduate Studies

Joseph J. Fedock — Joseph J. Fedock — 9/1/98
Date

STATEMENT OF PERMISSION TO USE

In presenting this thesis in partial fulfillment of the requirements for a master's degree at Montana State University-Bozeman, I agree that the Library shall make it available to borrowers under rules of the Library.

If I have indicated my intention to copyright this thesis by including a copyright notice page, copying is allowable only for scholarly purposes, consistent with "fair use" as prescribed in the U.S. Copyright Law. Requests for permission for extended quotation from or reproduction of this thesis in whole or in parts may be granted only by the copyright holder.

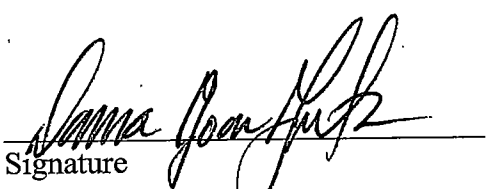

Signature

19 Aug 1998

Date

ACKNOWLEDGMENTS

First and foremost I would like to thank Prof. Timothy Minton for allowing me the opportunity to work on such an exciting project. From day one he showed a tremendous amount of enthusiasm for the science and an intense interest in designing and performing experiments. His willingness to help on even the worst tasks in the lab, take data for 15 hours straight, and assist in preparation of papers and talks (even the day before) created an excellent and thorough learning opportunity.

The experiments discussed in this thesis were carried out in Piero Casavecchia's lab in Perugia, Italy. I am very grateful to Piero, his group, Nadia Balucani and Michele Alagia, and Gian Gualberto Volpi for their generous hospitality and insight on the experiments.

My master's degree program was enhanced by the generosity of NASA's Marshall Space Flight Center. I would like to thank several individuals there, James Dowdy, James Zwiener, and Rachel Kamanetzky

I owe thanks to the other group members, James Seale and Jiaming Zhang, for making the lab and classes more fun. Good luck to you both.

My thesis advisor, Pat Callis, was always encouraging and I am grateful to him for his time and assistance. I would also like to thank Lee Spangler and David Singel.

Last but not least, I thank my parents, Jerry and Barb, my sisters, Dessa and Dana, and my grandfather, Bill Nixon, for all their love and support and making it possible for me to achieve all that I have. I hope they will join me in the road ahead.

TABLE OF CONTENTS

TABLE OF CONTENTS–Continued

LIST OF FIGURES

LIST OF FIGURES–Continued

ABSTRACT

Reactions of free radicals, such as atomic oxygen and chlorine, with gaseous saturated hydrocarbons have been studied extensively due to their importance in combustion and atmospheric chemistry, respectively. Such reactions of the ground state species are known to proceed through direct hydrogen abstraction mechanisms. The detailed dynamical information of these reactions in the gas phase, especially with chlorine, make them ideal systems to study in analogous reactions of these free radicals with hydrocarbon surfaces. The study of atomic oxygen with hydrocarbon surfaces has been pursued by the space community, as naturally occurring atomic oxygen in low Earth orbit readily reacts with and degrades polymer materials on the outer surfaces of spacecraft; however, the detailed dynamics of the interaction has remained elusive. The atomic chlorine reactions are ideal comparative systems because of the wealth of gas phase data available. In this thesis, reactions of atomic oxygen, ground and electronically excited, and atomic chlorine with a liquid hydrocarbon surface have been investigated with a crossed molecular beams apparatus in order to understand the initial interactions occurring at the surface. Additional experiments to study the steady-state interactions of atomic oxygen with a solid hydrocarbon surface were also investigated.

In Chapter 4, interactions of ground and electronically excited atomic oxygen with a continuously refreshed film of a long-chain saturated hydrocarbon, squalane ($C_{30}H_{62}$), are discussed. Angularly-resolved flux and energy distributions of reactively-scattered products revealed that the dominant volatile reaction product is the OH radical, which can be formed by an Eley-Rideal direct-abstraction mechanism, similar to the gas-phase reaction, or by a process that leads to trapping and desorption of the initial product. Both these processes occur with comparable probabilities. A second, surface-unique product, H_2O, is thought to be formed by abstraction of a hydrogen atom from the hydrocarbon chain by the primary OH product. The H_2O product also exits the surface through nonthermal and thermal mechanisms, although the thermal mechanism dominates. The $O(^1D)$ does not react to form a volatile reaction product and is believed to insert into the hydrocarbon chain, as observed in gas phase reactions. Steady-state reactions of atomic oxygen with a hydrocarbon surface result in the formation of volatile CO and CO_2, the end products of combustion, through thermal and nonthermal mechanisms.

A comparison of the dynamics of $Cl(^2P)$ and $O(^3P)$ reactions with a squalane surface is presented in Chapter 5. The only observable reaction product for the Cl reaction, HCl, was formed through two channels: 1) an Eley-Rideal direct abstraction mechanism, similar to observed $Cl(^2P)$ gas phase reactions and $O(^3P)$ reactions, and 2) thermal mechanism(s) not observed with oxygen. Construction of surface Newton Diagrams for the HCl and OH products allowed more specific comparison to gas-phase studies and a novel view of the role of the surface in these reactions.

CHAPTER 1

INTRODUCTION

Reactions of atomic oxygen with saturated hydrocarbons in the gas phase have been studied extensively over the past 40 years because of their importance in combustion. Early studies used kinetic data to infer the reaction mechanisms, while recent investigations have probed the reaction dynamics more directly. Oxygen atoms in the ground ^3P state react with a hydrocarbon by abstracting a hydrogen atom to form OH. Excited state O(^1D) may also abstract an H atom, but it is more likely that the O(^1D) atom will insert into a C–H bond to form an excited alcohol, which can be stabilized by collisions or can dissociate by C–C or C–O bond cleavage. Atomic chlorine undergoes H-atom abstraction reactions with saturated hydrocarbons analogous to those of O(^3P). Numerous investigations have focused on chlorine reactions with gaseous hydrocarbons because of their importance in atomospheric chemistry and various industrial processes. While a great deal is known about atomic oxygen and chlorine reactions with hydrocarbons in the gas phase, little is known about their reactions at hydrocarbon surfaces. When an oxygen or chlorine atom strikes a hydrocarbon surface a gas-phase-like H-atom abstraction reaction may occur, or the impinging atom may react less directly following multiple bounces or even trapping at the surface. Direct atom-abstraction and proton exchange reactions have been observed in molecular beam-surface

studies[1-6], but there are relatively few examples of such nonthermal reactions at the gas-surface interface. If abstraction reactions similar to those known to occur in gas-phase reactions, such as those involving atomic oxygen and chlorine, also occur at surfaces, then direct atom-surface reactions may be more common than previously thought. The goals of the work described herein are to develop a detailed picture of what happens when an oxygen or chlorine atom impinges on a hydrocarbon surface and to uncover the similarities and differences between these gas-surface reactions and analogous gas-phase reactions. The remainder of the introduction delves into atomic oxygen and chlorine reactions with hydrocarbons, the importance of these systems, known gas-phase dynamics, and possible surface effects.

Atomic Oxygen Reactions with Saturated Hydrocarbons

Atomic oxygen reactions with hydrocarbon surfaces are fundamental to most surface modifications of polymers. Oxygen plasma treatments are used, for example, to improve adhesion,[7] strip photoresists,[8] define patterns for microelectronics,[9] and enhance biocompatibility.[10] In the low Earth orbital space environment, atomic oxygen erodes thermal control and structural materials on the outer surfaces of spacecraft.[11] Plasma processing and materials testing for space durability are inherently complicated by the presence of a variety of reactive agents, such as excited-state neutrals, molecular oxygen, ions, and UV light. While the outcome of a plasma process may be optimized by trial and error regardless of the reactive species present, the validity of a materials test may be

compromised by interactions that are not representative of the space environment.[12] In either process, a knowledge of the mechanisms by which O atoms attack and degrade a hydrocarbon surface would improve efficiency by clarifying the relationship between process conditions and the resulting surface effect. Atomic oxygen in both the ground $O(^3P)$ and electronically-excited $O(^1D)$ states may be important reactants in environments used to modify and test hydrocarbon materials.

It might be assumed that an oxygen atom incident on a hydrocarbon surface would undergo abstraction and insertion reactions similar to those known to occur in the gas phase. Studies of the kinetics of $O(^3P)$ reactions with various saturated hydrocarbons in the gas phase have concluded that these reactions proceed by H-atom abstraction to form OH and alkyl radical products. Depending on whether the abstracted hydrogen atom is primary, secondary, or tertiary, the room-temperature rate constants (per H atom) are 5×10^{-16}, 7.2×10^{-15}, and 1×10^{-13} cm^3 $molecule^{-1}$ s^{-1},[13] the activation energies are 28.9, 18.8, and 13.8 kJ/mol, and the reaction exothermicities are −9.6, −29.3, and −43.1 kJ mol^{-1},[14] respectively. A crossed molecular beam experiment that employed laser-induced fluorescence detection of the OH product provided the first definitive proof of the abstraction mechanism.[14] Both this experiment and more recent dynamics studies,[15,16] where the OH product was detected, have shown that the reaction occurs primarily when the $O(^3P)$ atom is collinear with a C−H bond in the hydrocarbon molecule and that the reaction can be modeled well as the local interaction of an oxygen atom with a hydrogen atom attached to a structureless hydrocarbon fragment. In contrast to the $O(^3P)$ reactions, $O(^1D)$ has been thought to react either by H-atom abstraction or by insertion into a C−H bond. Cvetanović and coworkers have

investigated the kinetics of $O(^1D)$ reactions with various saturated hydrocarbons, and they found that the room-temperature rate constants were nearly gas kinetic, in the range 10^{-10} - 10^{-9} cm^3 $molecule^{-1}$ s^{-1}.[17] From their studies of $O(^1D)$ reactions with propane,[18] isobutane,[19] and neopentane,[20] they concluded that insertion leads to formation of an alcohol which may be stabilized at high pressures, while abstraction forms OH that persists at high pressure. The lifetime of the alcohol insertion product depends on the size and nature of the hydrocarbon and varies from 0.8 - 3 ps for CH_4[21] to ~4200 ps for $C(CH_3)_4$.[20] If the alcohol intermediate is not stabilized, then it will dissociate, with a strong propensity for C–C bond cleavage when the hydrocarbon is larger than CH_4. At both low and high pressures, the insertion products dominate. Dynamics studies by Luntz[22] and by Park and Wiesenfeld[23] have verified the existence of two competing reaction mechanisms through the identification of two populations of OH products, one with high internal excitation and the other with relatively little internal excitation. Luntz interpreted these results in terms of competing insertion and abstraction mechanisms, respectively. Park and Wiesenfeld instead suggested that internally hot OH arises from dissociation of short-lived insertion intermediates prior to energy equipartition, while the cold OH originates from dissociation of a long-lived insertion complex in which the internal modes have relaxed to the statistical limit. It should be noted, however, that recent experiments by Brouard and Simons[24] on the reaction of $O(^1D)$ with CH_4 found little evidence of bimodal character in the rotational populations of OH(v = 0). Intersystem crossing between singlet and triplet surfaces may lead to apparent abstraction reactions for $O(^1D)$ and insertion reactions for $O(^3P)$. Naaman et al. have proposed a singlet-to-triplet crossing mechanism to explain the observation of some of the

OH products in reactions of $O(^1D)$ with small clusters of CH_4 and C_3H_8.[25] Likewise, a triplet-singlet crossing mechanism can explain the stabilized cyclohexanol product detected in a crossed-beams study of the reaction of $O(^3P)$ with cyclohexane clusters.[26] Further evidence for triplet-singlet crossing to form an insertion product comes from Patiño et al., who reported that reactions of liquid saturated hydrocarbons with $O(^3P)$ in an oxygen plasma yield secondary alcohols and ketones.[27]

Atomic Chlorine Reactions with Saturated Hydrocarbons

Reactions of atomic chlorine with hydrocarbon surfaces are virtually unknown; however, the dynamics of Cl-atom reactions with hydrocarbons in the gas phase have been studied in depth. In fact, the understanding of Cl-atom reaction dynamics with gas-phase hydrocarbons is even deeper than that of the analogous O-atom reactions. The relative wealth of knowledge about atomic chlorine reactions with hydrocarbons arises from the fact that this system is fairly simple, making the experiments easier to perform and interpret. For, example, the chlorine atom can easily be prepared in one spin state, ^2P, and the only direct reaction product is HCl. Thus, atomic chlorine is an ideal reactant for our studies of gas-surface reactions, where a prime goal is to relate gas-surface and gas-gas reaction dynamics. Furthermore, the close analogies between reactions of Cl with hydrocarbons and O with hydrocarbons allow us to strengthen our understanding of atom-surface reactions by comparing the reaction dynamics of both these species with a hydrocarbon surface.

Kinetic and theoretical studies of reactions of atomic chlorine with gaseous alkanes

confirm that the reactions occur through a direct abstraction mechanism with a linear transition state, similar to the preferred geometry of $O(^3P)$ reactions.[28-30] The rate constants are gas kinetic and increase as the hydrocarbon molecule increases in complexity. Reactions of atomic chlorine with methane, ethane, and isobutane to form HCl have rate constants of 2×10^{-11}, 9×10^{-11}, and 1×10^{-10} cm^3 molecule^{-1} s^{-1}, respectively.[29, 31] This trend is consistent with the increasing reactivity of primary, secondary, and tertiary hydrogen atoms. Additionally, the reactions of Cl with methane and ethane, which contain only primary hydrogen atoms, are endothermic by about 7.2 and 11.1 kJ mol^{-1}, respectively,[32,33] while the reactions of Cl with all larger alkanes, containing secondary and tertiary hydrogen atoms, are slightly exothermic. For example, propane is exothermic by 6 kJ mol^{-1} if a primary hydrogen atom is abstracted and 22 kJ mol^{-1} if a secondary hydrogen atom is abstracted.[34] The rate constants are temperature independent for alkanes with three or more carbons, indicating little or no barrier to reaction.[29,31] For chlorine atom reactions with methane, the barrier is about 10 kJ mol^{-1}.[31] The barrier to reaction is believed to approach zero as the hydrocarbon becomes more complex.[31]

A number of dynamical investigations of atomic chlorine reactions with alkanes have shed further light on the details of the gas-phase reaction mechanisms. Zare and coworkers and Varley and Dagdigian have used resonance enhanced multiphoton ionization (REMPI) and core extraction techniques to investigate hydrogen abstraction mechanisms from small hydrocarbons.[34-41] Reactions of chlorine with ground-state methane led to HCl products that were rotationally cold, which scattered in the backward direction with respect to the center-of-mass (c.m.) velocity of the Cl reactant.[38] The combination of cold rotational populations

and strong backward scattering implies a tightly constrained linear transition-state complex which is formed through a limited cone of acceptance (small impact parameters). An analogous conclusion was reached in studies of $O(^3P)$ reactions with alkanes. Further investigations by Zare et al. on the reaction of atomic chlorine with vibrationally-excited methane, $CH_4(v_3=1)$ revealed an increase in reaction cross section relative to the reaction with ground-state methane.[36] They found that 70 percent of the HCl product was formed in the ground vibrational state, which was scattered predominantly in the backward direction, as in the reactions with ground state methane. The HCl(v=0), formed in the reaction with vibrationally excited methane, showed greater rotational excitation. This observation was interpreted as the additional energy in the methane reactant allowing some degree of relaxation from the collinear intermediate geometry. The vibrational energy of the methane provides energy along the reaction coordinate, allowing larger impact parameter collisions to have sufficient energy to lead to reaction. The remaining 30 percent of HCl product was formed in the first excited state and was found to have two populations. The component having lower rotational excitation was scattered predominantly in the forward direction. The second component, with higher rotational excitation, tended to scatter in the backward direction. The backward-scattered component reached an intensity comparable to the forward-scattered component for $J = 3$. The more forward-scattered HCl($v = 1, J$) products are the result of a stripping mechanism, where the Cl approaches the C–H bond more perpendicular (large impact parameters) and there is a relatively weak interaction. Smaller impact parameter collisions lead to stronger interactions, with products that are scattered in the backward and sideways directions and that show rotational excitation as a result of an

impulsive kick as the initial velocity is redirected. Relaxation of the collinear intermediate was also seen in the reaction of Cl with ethane.[37] Hydrogen abstraction from ethane by Cl atoms gave an HCl product distribution that was essentially isotropic. This observation was explained in terms of the reduced barrier to reaction for ethane.

The effect of hydrogen atoms in different environments on the dynamics of hydrogen-atom abstraction by atomic chlorine appears to be more important in alkane reactions with atomic chlorine than in the corresponding atomic oxygen reactions. Reactions of atomic chlorine with selectively deuterated propane showed that secondary hydrogen atoms were abstracted preferentially to primary hydrogen atoms (consistent with rate data), and the primary H atoms were predominantly backward-scattered while the secondary H atoms were scattered more isotropically.[34,42] The rotational excitation of the HCl product from abstraction of a secondary H atom was found to be higher than the HCl product from abstraction of a primary H atom. In a crossed molecular beam study of the Cl reaction with propane employing detection of the propyl radical using VUV synchrotron radiation photoionization, Blank and coworkers identified two mechanisms that gave rise to a forward-scattered propyl component and a backward-and-sideways scattered propyl component.[43] The spectator-stripping (high impact parameter, forward scattering) mechanism was observed for abstraction of both secondary and primary hydrogen atoms at higher collision energies (31.6 kJ mol^{-1}). At lower collision energies, the propyl radicals formed through the loss of the primary hydrogen atoms were backwards-scattered, while the loss of the secondary hydrogen atoms showed an isotropic scattering distribution of the propyl radical. Similar scattering phenomena were reported in a study of the reaction of Cl atoms with

selectively deuterated isobutane, which contains tertiary hydrogen atoms.[41] The abstraction of the tertiary D atoms led to more sideways-scattered DCl products than observed with the reactions with secondary hydrogens. The backward-scattered nature of the HCl product from abstraction of a primary hydrogen atom indicates a more restrictive linear geometry of the intermediate while the diffuse scattering from the secondary and tertiary hydrogens indicates a relaxation of the requirement for collinear geometry. The barriers to reaction calculated for propane and isobutane are small, a few kJ mol^{-1}, and are consistent with these results since there is only a small energy requirement along the reaction coordinate, allowing larger impact parameter collisions to lead to reaction.

Surface Effects

The reactions of atomic oxygen and chlorine at a hydrocarbon surface may have additional reactive pathways. While gas-phase-like reactions, such as abstraction of an H atom, by Cl or $O(^3P)$, or insertion of $O(^1D)$ into a C–H bond, might occur, the consequences of these initial reactive events are likely to be different on a surface. In the atomic oxygen reactions, for example, the OH product could desorb immediately or it could react further to form H_2O, which would then desorb. It is very likely that reactions on the oxygen singlet potential energy surface would not lead to volatile products if the alcohol intermediate were stabilized at the hydrocarbon surface. Atomic chlorine may become trapped, react, and then desorb as HCl. The reactions will depend sensitively on the atom-surface interaction dynamics. Desorption kinetics, surface structure, reactivity of transient species, and energy

transfer at the surface will affect the probability of the various possible reactive pathways. Analogy with gas-phase reactions simply does not provide all the information necessary to understand even the initial reactions at a hydrocarbon surface.

Overview of Thesis

This thesis mainly describes an investigation into the dynamics of the reactions of gaseous oxygen and chlorine atoms with a continuously-refreshed saturated hydrocarbon surface. The use of such a surface isolates this study to the initial reactions that occur when a hydrocarbon surface is subjected to atomic oxygen or chlorine attack. An atomic oxygen beam, containing both $O(^3P)$ and $O(^1D)$, and an atomic chlorine beam were directed at the hydrocarbon surface, and the volatile products were detected. From the dynamical behavior of these products, we inferred the reactive processes that took place at the surface. The hydrocarbon, squalane, was used in its liquid phase at room temperature. Squalane molecules contain primary, secondary, and tertiary hydrogen atoms and are believed to orient preferentially with their chain ends at the liquid surface.[44] Thus, initial attack will favor primary H atoms on methyl groups. Reaction with methyl groups provides the best opportunity to look for possible volatile products of an $O(^1D)$ insertion reaction that leads to C–C bond fission and subsequent liberation of CH_2OH (or CH_3O). This is the only plausible direct reaction that would lead to loss of carbon from the surface.

Reactions of atomic oxygen with a solid polypropylene surface were also investigated. The solid surface was placed under continuous oxygen atom attack in order to study the

steady state reactions that occur at the surface and identify the material removal mechanisms of a polymer that is undergoing etching by atomic oxygen. The results presented are preliminary, but they do confirm that CO and CO_2 are the dominant carbon-containing products during etching, and they reveal that these products exit the surface via two distinct mechanisms.

The following chapter (Chapter 2) describes the experimental details, including the experimental configuration, the preparation of beams of atomic oxygen and chlorine, and the nature of the data that were collected.

Chapter 3 contains a presentation of representative experimental results and a description of the analysis that was performed.

A discussion of the results is presented in Chapters 4 and 5. Chapter 4 focuses on the reaction dynamics of atomic oxygen with the hydrocarbon surface, while Chapter 5 provides a discussion of the dynamics of the reaction of atomic chlorine with the hydrocarbon surface and gives a comparison with the atomic oxygen reaction dynamics.

CHAPTER 2

EXPERIMENTAL METHODS

Experimental Configuration

The experiments were performed with a crossed molecular beams apparatus[45] (see Fig. 2-1). A high-pressure radio frequency discharge source[46] was used to produce continuous supersonic beams of oxygen and chlorine atoms. These beams were directed at a hydrocarbon surface, and scattered products were detected with a rotatable mass spectrometer detector. The rotation axis of the detector was coincident with the axis of rotation of the surface, and the surface normal was contained in the detector rotation plane. A pseudorandom chopper wheel[47] was used to modulate the products in order to allow determination of their translational energy distributions.

The beam exited the differentially-pumped source chamber through a conical skimmer and passed through an ion deflecting field of approximately 500 V cm^{-1} and a second defining aperture (collimator) before impinging on the surface. The total distance from the nozzle to the surface was 87.6 mm. At the surface, the beam had an angular divergence of 1.6° and a diameter of 2.5 mm. The pressure in the main scattering chamber was maintained near 5×10^{-7} Torr while the beam was running.

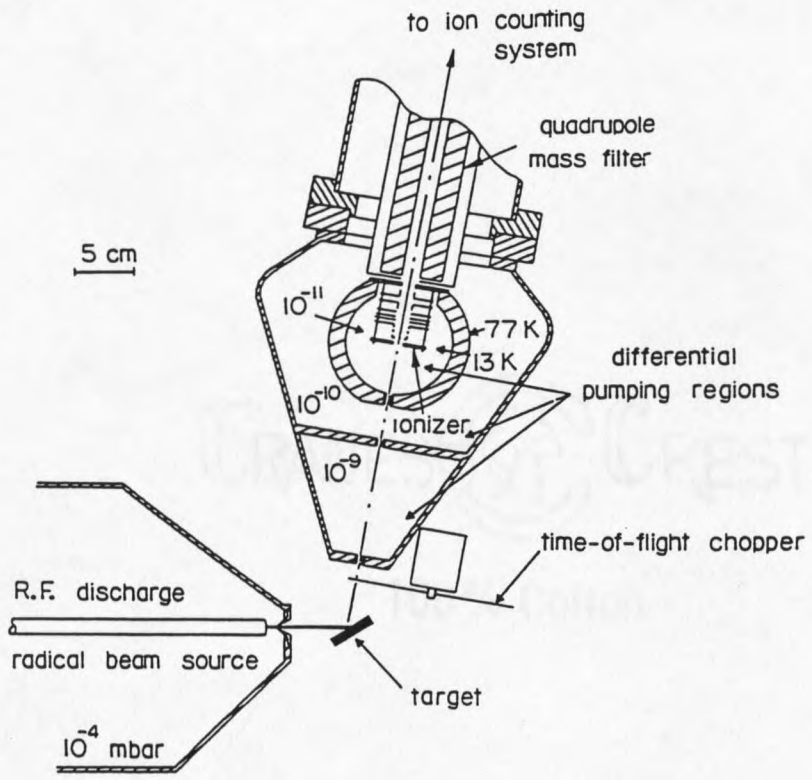

Figure 2-1. Schematic diagram of the atomic oxygen beam source, the differentially-pumped scattering region containing the target surface, and the rotatable mass spectrometer detector.

Products that scattered from the surface passed through the pseudorandom chopper wheel, located 4.3 cm from the collision center on the surface, and then traveled 23.0 cm from the wheel to the electron bombardment ionizer in the detector. A quadrupole mass filter was used in conjunction with an electron multiplier for ion detection. The ion signal was collected with a multichannel scaler. Various rotation speeds of the chopper wheel were used, which gave resolution in the resulting time-of-flight (TOF) spectra in the range of 5 - 10 μs channel^{-1}.

Incident Beams

The incident oxygen beams contained atomic and molecular oxygen, with the atomic fraction approximately 70 percent. Translational energy distributions of the species in the beam were obtained by aligning the beam and detector axes (with the surface lowered out of the beam path) and collecting TOF distributions with the use of the pseudorandom chopper wheel or a "single-shot" slotted disk chopper. While the atomic component of the beam is mostly ground-state $O(^3P)$ atoms, it also contains a small percentage (<10%) of metastable $O(^1D)$ atoms.[48] The fraction of $O(^1D)$ in the beam may be varied by adjusting beam conditions, such as feed gas mixture, RF power, and operating pressure. Beam energies are also controlled by source operating conditions.

The liquid experiments were conducted with two operating conditions that led to average translational energies of 47 and 21 kJ mol^{-1}. In order to search for a specific contribution of $O(^1D)$ reactions to the observed signals, we used a third set of operating conditions, including increasing the percentage of O_2 in the feed gas from 5 to 15 percent, which yielded an average O-atom translational energy of 47 kJ mol^{-1}. Based on reactive scattering studies of similar He- and Ne-seeded beams with H_2S, the $O(^1D)/O(^3P)$ ratio in the beam was estimated to be on the order of 0.05, and this ratio was estimated to decrease by 40 percent on going from the 5% O_2/He to the 15% O_2/He beams.[49] Source operating conditions and resulting O-atom translational energy distributions are presented in Fig. 2-2. The incident O-atom flux at the surface was on the order of 10 -100 monolayers s^{-1}.

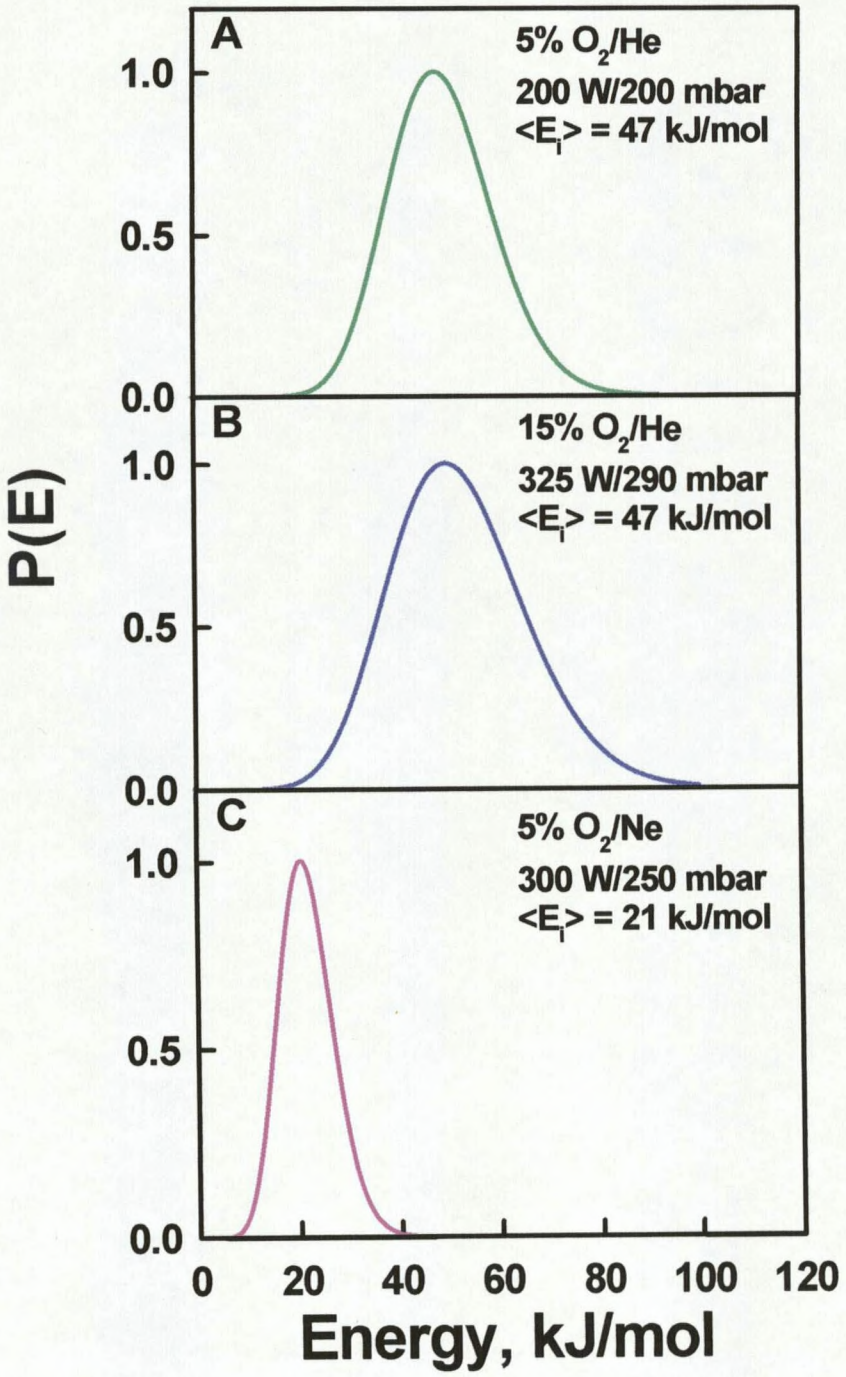

Figure 2-2. Translational energy distributions of the atomic oxygen component of three beams that were used. Each panel contains the feed gas mixture, the RF operating power, the source stagnation pressure, and the average O-atom translational energy. Unless otherwise specified, all data collected with an incident energy of $\langle E_i \rangle$ = 47 kJ/mol correspond to the incident beam whose translational energy distribution and operating conditions are shown in **A**.

Experiments with a solid (polypropylene) target surface utilized slightly different beam conditions that led to an average O-atom translational energy of 61 kJ mol^{-1} in the incident beam. The energy width (FWHM) of this beam was approximately 75 kJ mol^{-1}.

Beams of atomic chlorine with average translational energies of 118 and 47 kJ mol^{-1} were produced by altering the source feed-gas and operating conditions of the source. The feed-gas mixture used for the higher-energy beam was Cl_2 (2%), O_2 (2%), and He (96%), and the mixture used for the lower-energy beam was Cl_2 (2.75%), O_2 (2.75%), and Ne (94.5%). The source operating conditions were 250 mbar/300 W or 245 mbar/300 W for the higher- and lower-energy beams, respectively. The fraction of undissociated chlorine in the beams was approximately 10 percent.

Hydrocarbon Surfaces

The liquid hydrocarbon that served as the reactive collision partner for most of the experiments with the atomic oxygen and chlorine beams was squalane (2,6,10,15,19,23-hexamethyltetracosane), which is a liquid with a vapor pressure at room temperature of 2×10^{-8} Torr. Before placement in the vacuum chamber, the squalane sample was degassed under vacuum for more than 12 hours at 50°C. A continuously-refreshed film of squalane was produced by rotating a polished stainless steel wheel through a liquid reservoir[50] held at 25°C. The film on the wheel was cleaned by passing the wheel by a sapphire scraper, leaving a fresh 100 μm film on the wheel prior to exposure by the atomic beam. The rotation rate was 0.21 Hz; thus the beam intercepted the film for 0.24 s.

The solid hydrocarbon used to study the material removal processes under steady-state etching conditions with atomic oxygen was atactic polypropylene. The sample was prepared by dissolving the polypropylene in hexane and spin coating a 100 μm thick coating on a silicon disk. The thickness was verified with a scanning electron microscope. The sample remained at room temperature throughout the experiment.

Observed Signals

In the atomic-oxygen experiments, both hydrocarbon surfaces showed inelastic scattering signals at mass-to-charge ratios (*m/z*) of 16 (O^+) and 32 (O_2^+). Reactive product signals were only detected at *m/z* = 17 (OH^+) and 18 (H_2O^+) for the liquid surface, while additional signals at *m/z* = 28 (CO^+) and 42 (CO_2^+) were detected from the solid. Typical integrated counting rates were approximately 160 s^{-1} and 90 s^{-1} and were dependent on the incident and detection angles. In the atomic chlorine experiment, signals were observed at *m/z* = 37 (Cl^+) and 38 (HCl^+), corresponding to inelastic and reactive scattering, respectively. Counting times varied from 600 to 3600 s. TOF distributions were collected for three incident angles, 30°, 45°, and 60°. A range of detection (final) angles was used for each incident angle, but the sum of the incident and final angles always fell in the range 70°-105°. All angles are given with respect to the surface normal.

The potential of two by-products formed in the beam source -- ultraviolet light and ions -- to be involved in the surface reactions was considered. The ions were almost entirely removed during the experiment by the ion deflecting field. In addition, the TOF distributions

of the reactive product signals were unchanged when the ion deflecting field was turned off. The possible effect of the ultraviolet light was tested with the use of a double chopper wheel (consisting of a slotted disk and a second disk with tabs aligned with the slots in the first disk) that acted as a low-resolution velocity selector which passed a beam pulse but was opaque to light. The double chopper wheel arrangement was placed in the path of the incident beam, and for this test, the pseudorandom chopper wheel in front of the detector was removed. TOF distributions detected at m/z = 17, 18, and 38 collected with the double chopper wheel (no light) were identical to those collected with the single slotted disk (light). The ultraviolet light from the source therefore appears to have had no measurable effect on the surface reactions.

CHAPTER 3

RESULTS AND ANALYSIS

Atomic Oxygen Reactions

Figures 3-1 through 3-3 show representative TOF distributions for $m/z = 16$, 17, and 18, respectively, that were collected at a detector angle of 45° when the atomic oxygen beam impinged, at the two different incident energies, on the squalane surface at an incident angle of 60°. The shapes of the TOF distributions depended on the incident and final angles; however, all TOF distributions appeared to be bimodal.[51] We deconvoluted the bimodal distributions by assuming that the slow component corresponded to products that were in thermal equilibrium with the surface and therefore exited the surface with a Maxwell-Boltzmann (M-B) distribution of velocities. The difference between an overall TOF distribution and the assumed M-B component was taken to be the TOF distribution of the second, hyperthermal, component, which corresponds to products that exited the surface before thermal equilibrium was established.

The TOF distributions of OH and H_2O products following reaction of O atoms with polypropylene were very similar to those observed in the reaction with squalane. However, reaction with stationary polypropylene led to additional large signals at m/z = 28

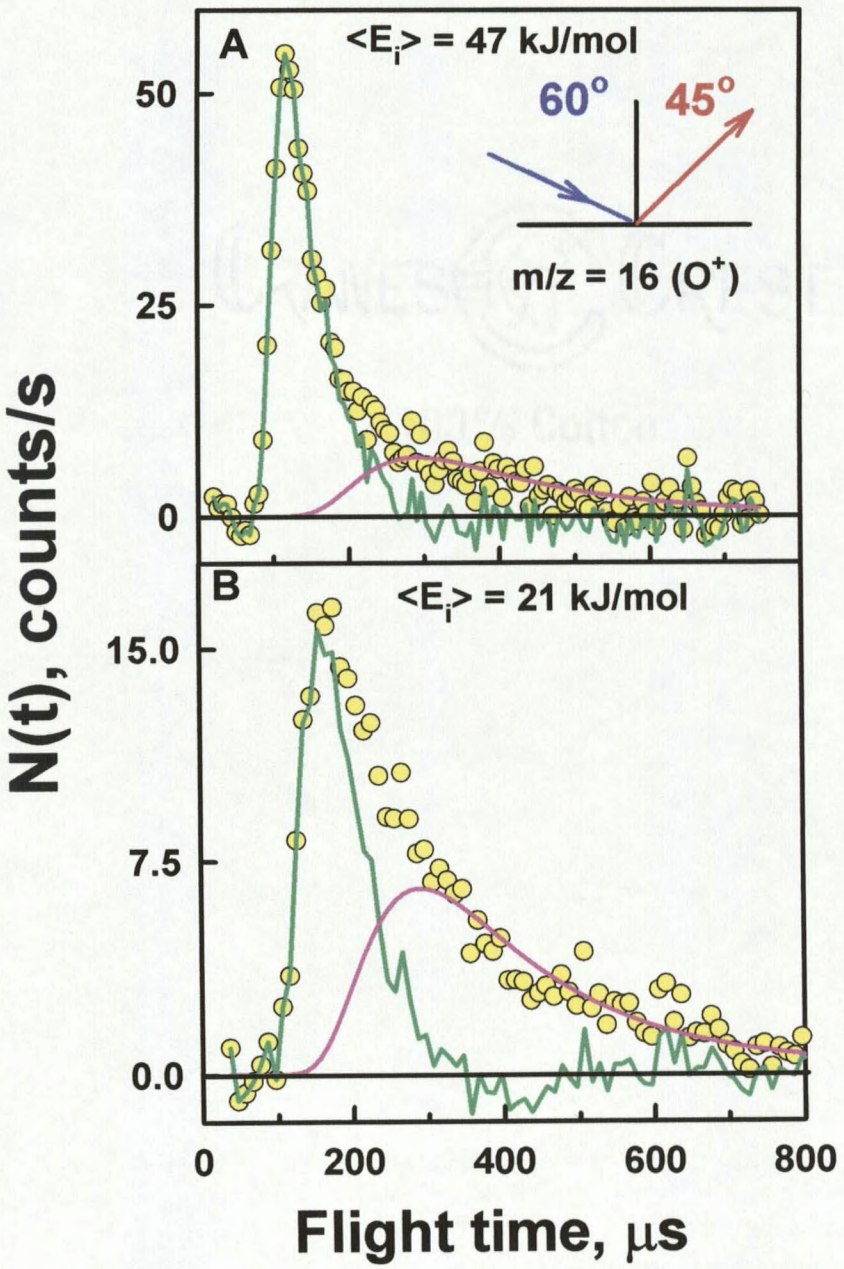

Figure 3-1. Representative time-of-flight distributions for oxygen atoms scattering from a squalane surface following impact at two incident energies and incident and final angles of 60° and 45°, respectively. Two populations of scattered atoms are identified, corresponding to inelastic scattering (fast) and trapping desorption (slow). The pink curves represent the thermal (Maxwell-Boltzmann) components, and the green curves represent the hyperthermal components, which come from the difference between the overall distributions and the thermal components.

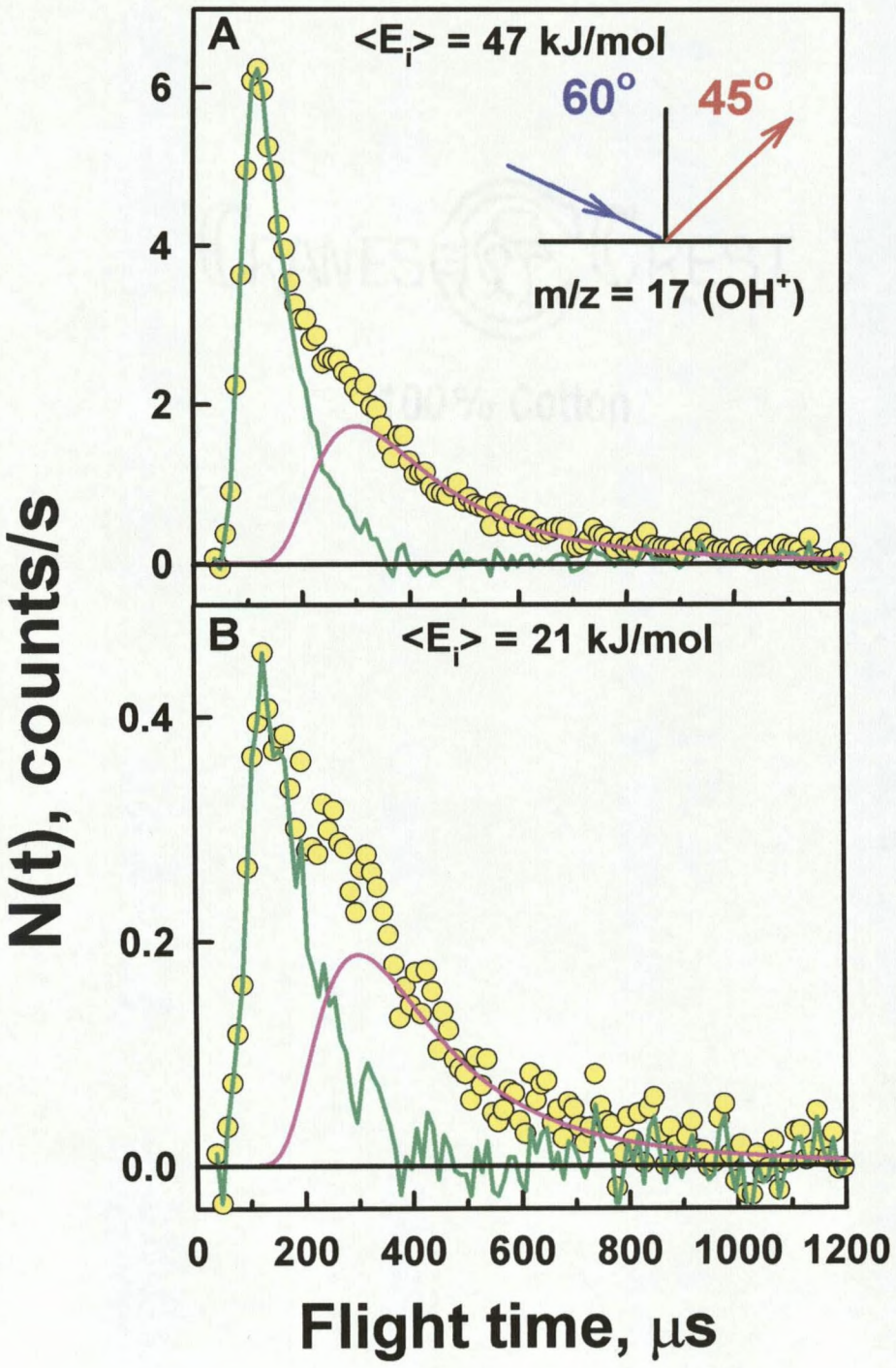

Figure 3-2. Representative time-of-flight distributions of OH products following reaction of oxygen atoms with a squalane surface at two incident energies and incident and final angles of 60° and 45°, respectively.

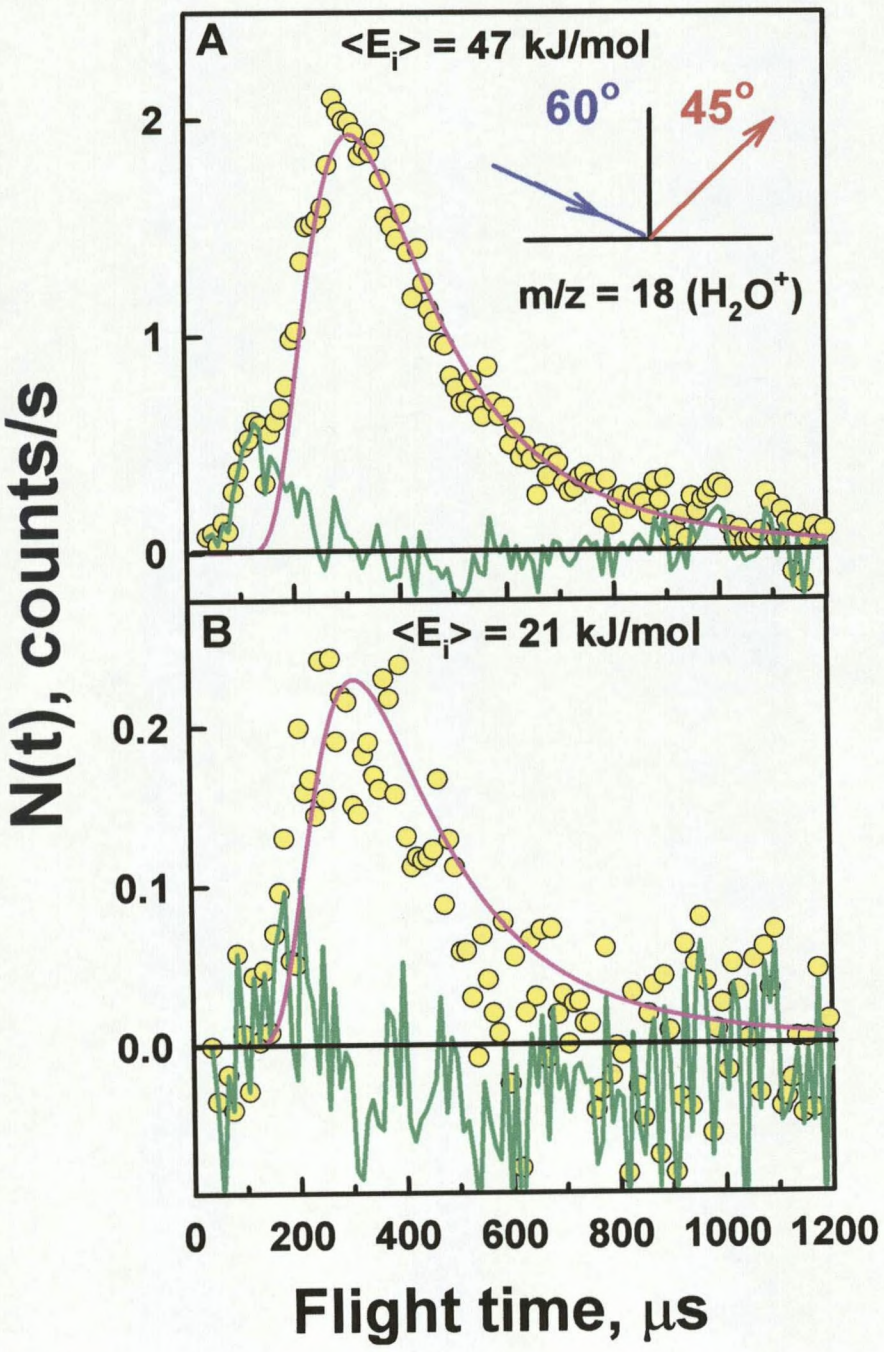

Figure 3-3. Representative time-of-flight distributions of H_2O products following reaction of oxygen atoms with a squalane surface at two incident energies and incident and final angles of 60° and 45°, respectively.

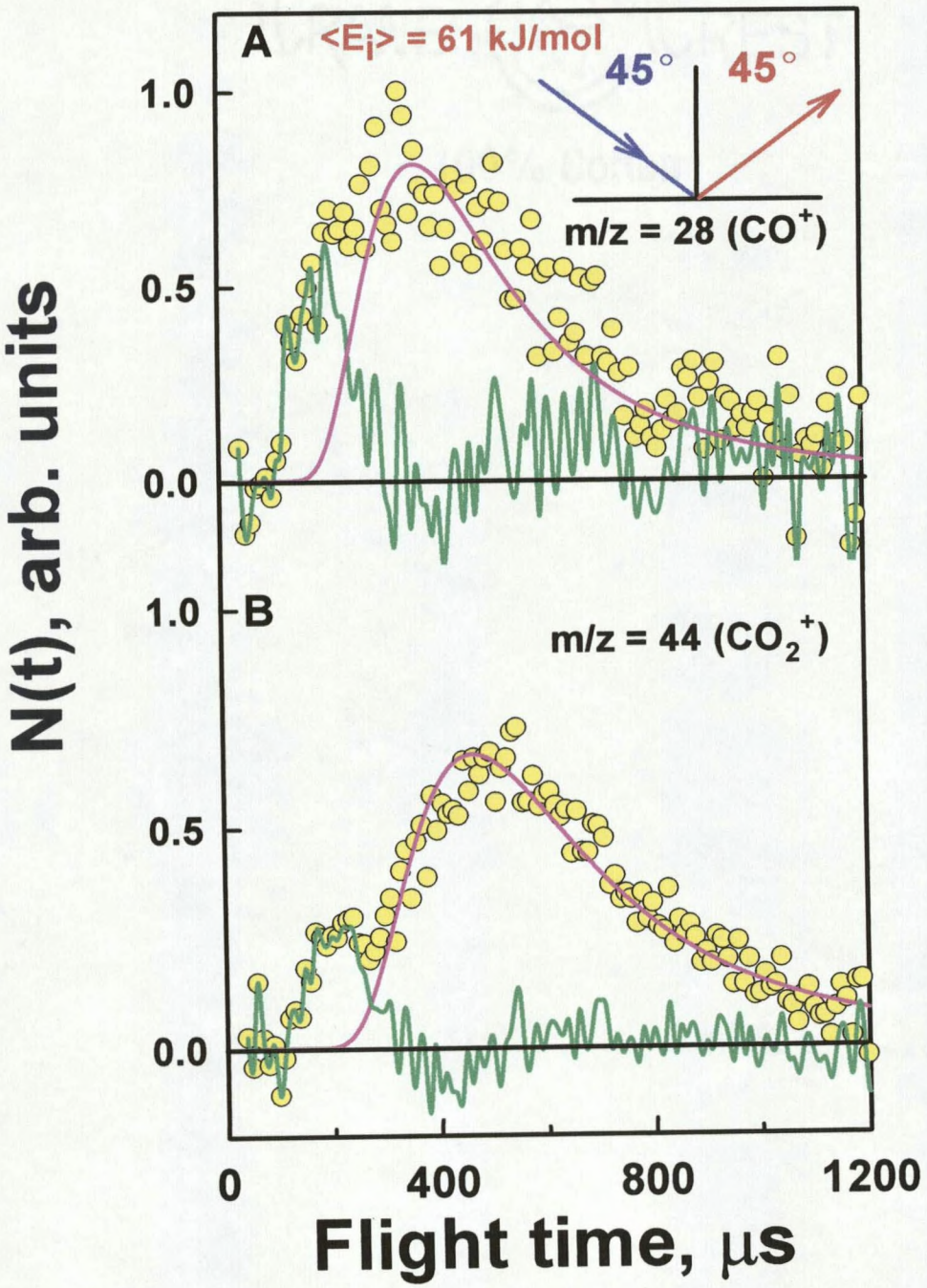

Figure 3-4. Representative time-of-flight distributions of CO (panel **A**) and CO_2 (panel **B**) product liberated from the polypropylene surface following reaction with a 61 kJ/mol atomic oxygen beam with incident and detected angles of 45°.

(CO^+) and 44 (CO_2^+). Figure 3-4 shows representative TOF distributions for the CO and CO_2 reactive products. The signals detected at m/z = 28 and 44 appear to contain at least two components, one thermal and the other hyperthermal.

The respective translational energy distributions that were derived from the TOF distributions in Figs. 3-1 through 3-3 are shown in Figs. 3-5 through 3-7. The hyperthermal distributions are broad, indicating a wide range of energy transfers with the surface, whether a reaction occurs or not. The high-energy tails of the O and OH distributions fall to zero near the maximum available energy, which is the highest translational energy of the incident beam distribution for inelastic scattering and the highest beam energy (40 or 80 kJ/mol for the lower and higher energy beams, respectively) plus the reaction exothermicity ($-\Delta H$ = 9 - 43 kJ/mol, depending on which type of H atom is abstracted) for reactive scattering to produce OH. Both the TOF distributions and the corresponding translational energy distributions show that the average final energies of the hyperthermal components increase when the incident energy is increased. In general (not shown), the final energies of the hyperthermal components increase for more grazing collisions.

Representative angular distributions of the two components of scattered O and OH flux for $\theta_i = 60°$ and $\langle E_i \rangle = 47$ kJ mol^{-1} after scattering from the squalane surface are shown in Fig. 3-8. The angular distribution for the thermal component follows a $\cos\theta_f$ distribution, while the angular distribution for the hyperthermal component has a maximum at $\theta_i = 40°$ and is much narrower than a cosine distribution, as seen by the good match of a $\cos^4(\theta_i - 37°)$ function to the observed data. For all detected products at all incident angles and energies, the thermal component exhibited a cosine angular distribution, while the

hyperthermal component tended to have a narrower angular distribution with a maximum at angles greater than $\theta_i = 0°$.

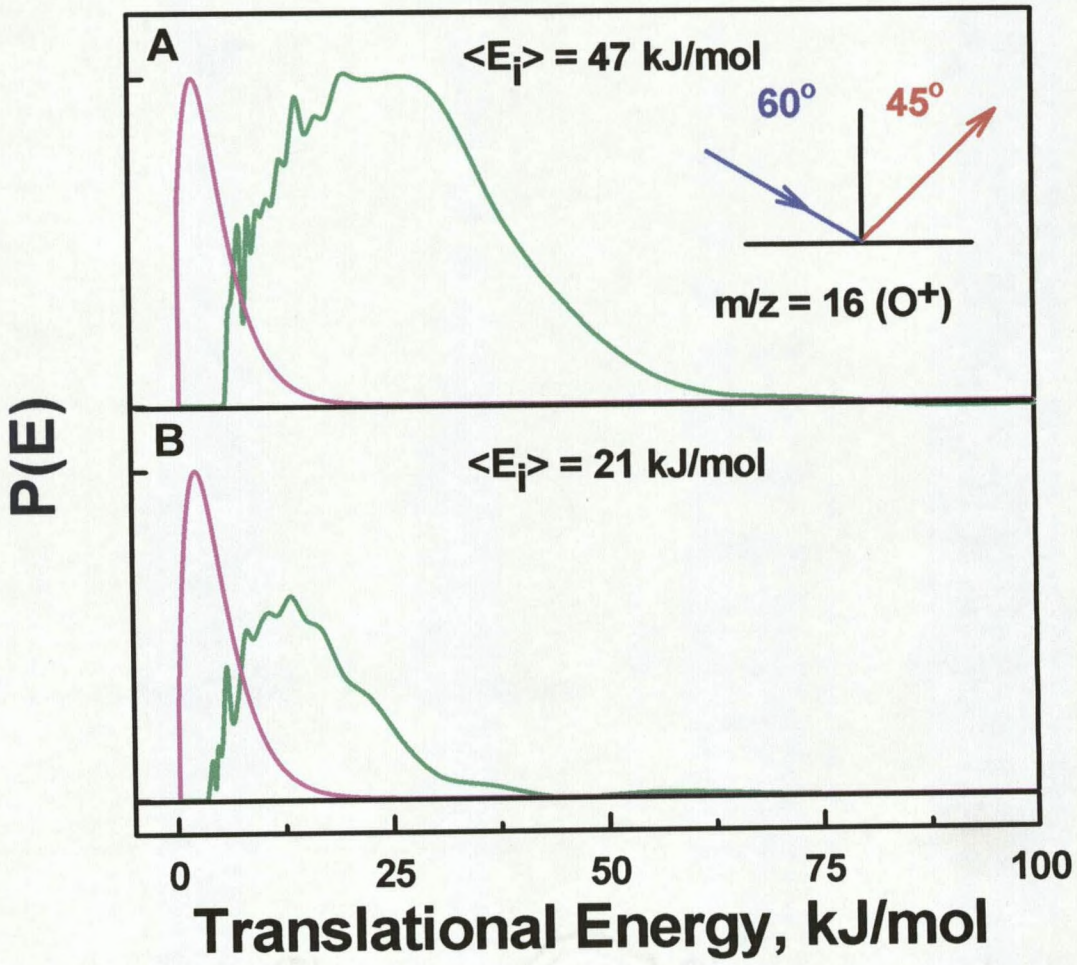

Figure 3-5. Translational energy distributions of scattered oxygen atoms derived from the time-of-flight distributions in Fig. 3-1. Each panel shows thermal (pink) and hyperthermal (green) components. The noise on the hyperthermal component arises from the noise in the data, which is transferred by the direct inversion of the time-of-flight distribution to a translational energy distribution.

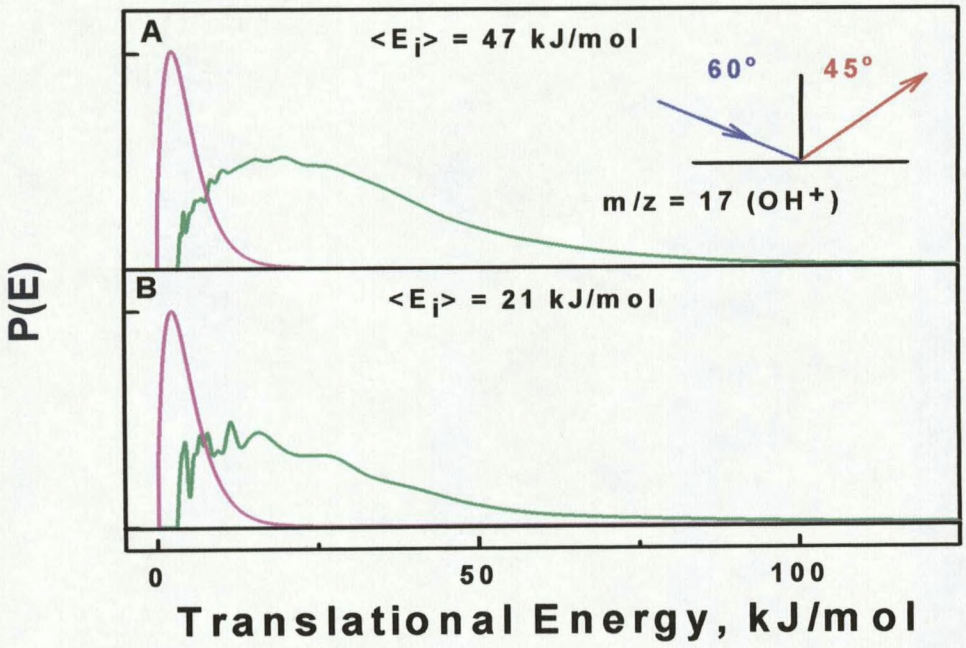

Figure 3-6. Translational energy distributions of reactively-scattered OH derived from the time-of-flight distributions in Fig. 3-2. Each panel shows thermal (pink) and hyperthermal (green) components.

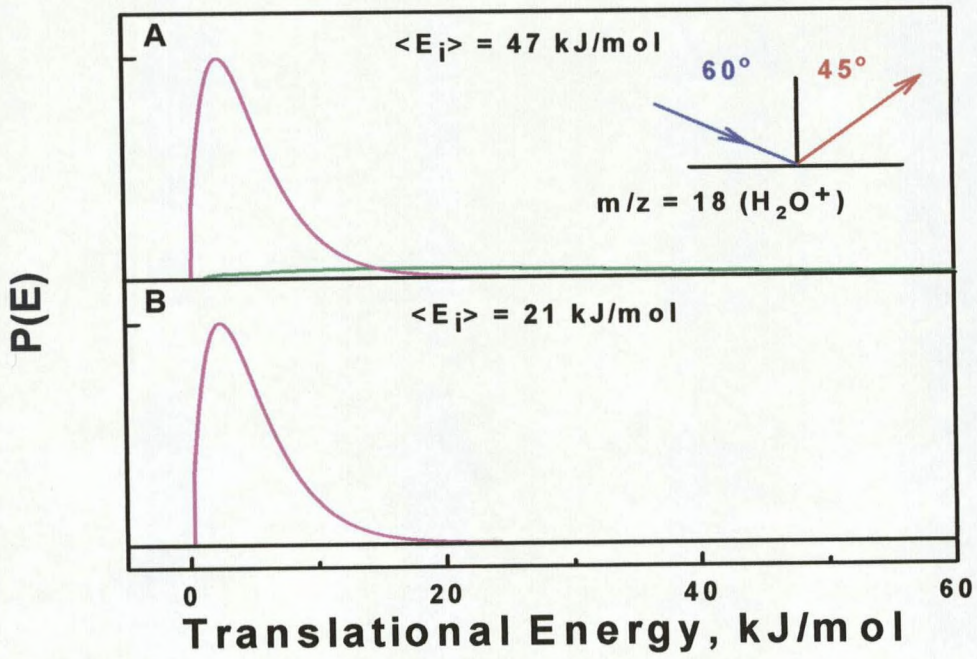

Figure 3-7. Translational energy distributions of reactively-scattered H_2O derived from the time-of-flight distributions in Fig. 3-3. The top panel shows thermal (pink) and hyperthermal (green) components, while the bottom panel shows only the thermal component. In this figure, the hyperthermal component has been smoothed.

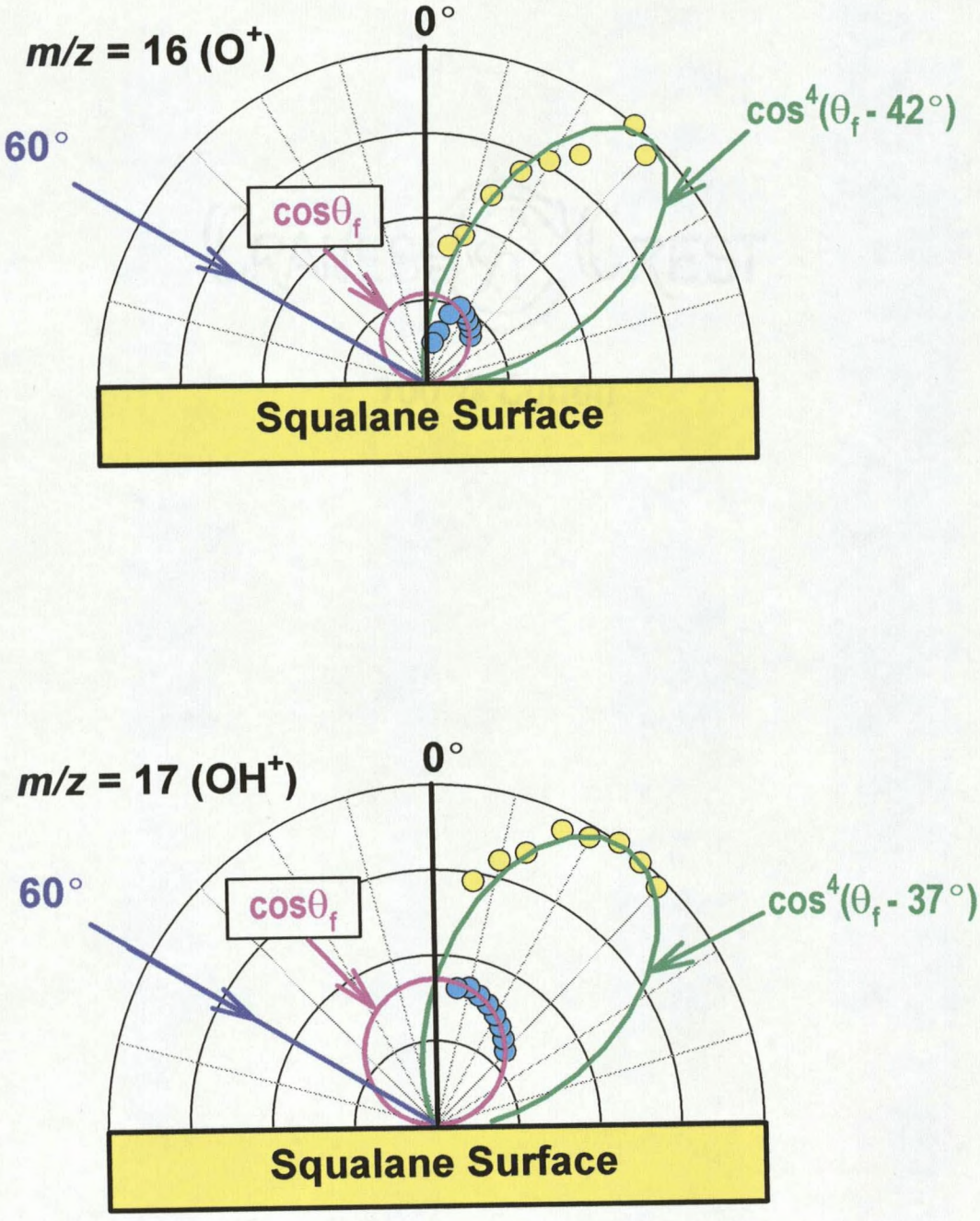

Figure 3-8. Angular distributions of inelastically scattered O flux and reactively-scattered OH flux, separated into thermal and hyperthermal components. The thermal signals follow a cosine distribution about the surface normal, while the hyperthermal signals have a distribution that is much narrower than cosine, with a maximum near $\theta_f = 40°$ for both species.

TOF distributions of OH products scattered from the squalane surface were collected with the atomic oxygen beam operating under two different conditions that yielded the same average incident energy of 47 kJ mol^{-1}. The two distributions collected for $\theta_i = 60°$ and $\theta_f = 45°$ are shown in Fig. 3-9. These distributions are identical within the signal-to-noise limits of the data. Even though the two incident O-atom beams had slight but measurably different average energies and distributions, there was no detectable difference in the two OH product TOF distributions generated with each beam. Not only did the range of final energies exceed the energy width of the incident O-atom beam, but the energy resolution at the fast edge of the TOF distributions was not sufficient to reveal any differences in flight time arising from the slightly different incident beam distribution.

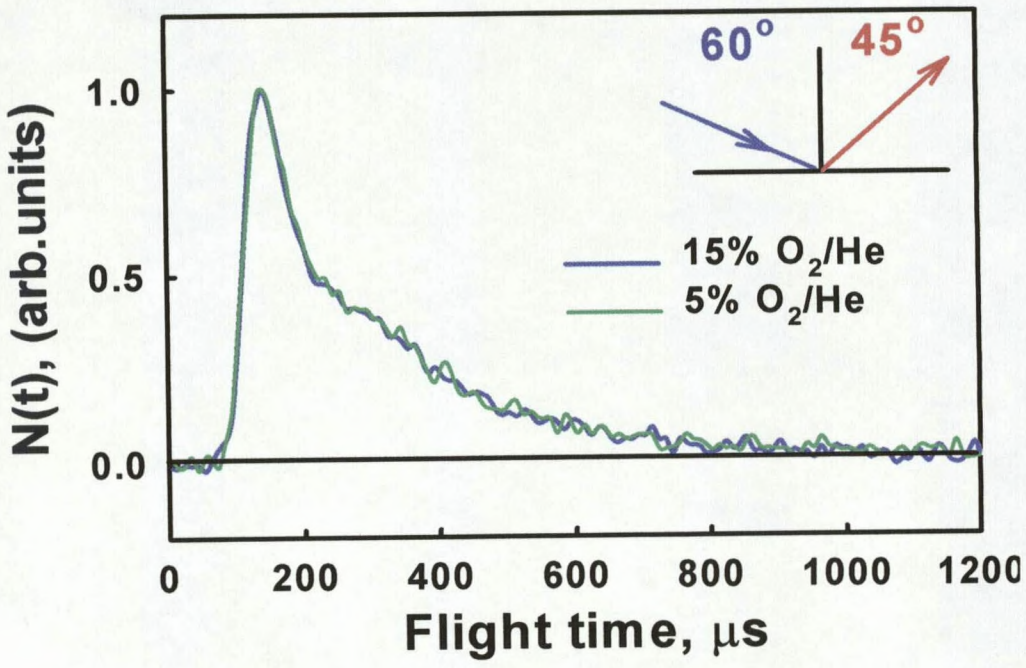

Figure 3-9. Time-of-flight distributions of OH products following impingement on a squalane surface of two different atomic oxygen beams with the same average O-atom translational energy of 47 kJ/mol (refer to Fig. 3-2). Within the signal-to-noise and time-resolution limitations of the data, the shapes of these distributions are identical.

Atomic Chlorine Reactions

Fig. 3-10 shows TOF distributions for m/z = 37 (Cl^+) that were collected at detector angles of 45°, 25°, and 10° when the atomic chlorine beam impinged, at an incident energy of 118 kJ mol^{-1}, on the squalane surface at an incident angle of 60°. Ionizer fragmentation of residual Cl_2 in the beam to produce Cl^+ was not corrected for in these TOF distributions. TOF distributions of the reactively scattered product, HCl, collected under the same conditions, are shown in Fig. 3-11. All the distributions are bimodal and were deconvoluted by assuming the slow component can be described by a Maxwell-Boltzmann distribution, as discussed earlier in this chapter. The effective surface temperatures were 500 K for the m/z = 37 data and 350 K for the m/z = 38 data. Both inelastic and reactive scattering TOF distributions contain thermal and hyperthermal components. The thermal component is much more dominant in the TOF distribution for HCl^+ than for the Cl^+ TOF distribution, although the HCl^+ distribution still has a significant hyperthermal signal. The TOF distributions of Cl^+ and HCl^+ collected following impingement of the lower-energy beam, with an incident angle of 60° and a detected angle of 45°, are shown in Fig. 3-12. Again, both inelastic and reactive scattering signals are bimodal.

The respective translational energy distributions that were derived from the higher energy TOF distributions are shown in Figs. 3-13 through 3-14. As in the reaction of O atoms with squalane, there is a broad range of energy transfers in the hyperthermal components of Cl and HCl distributions. The translational energy distribution of

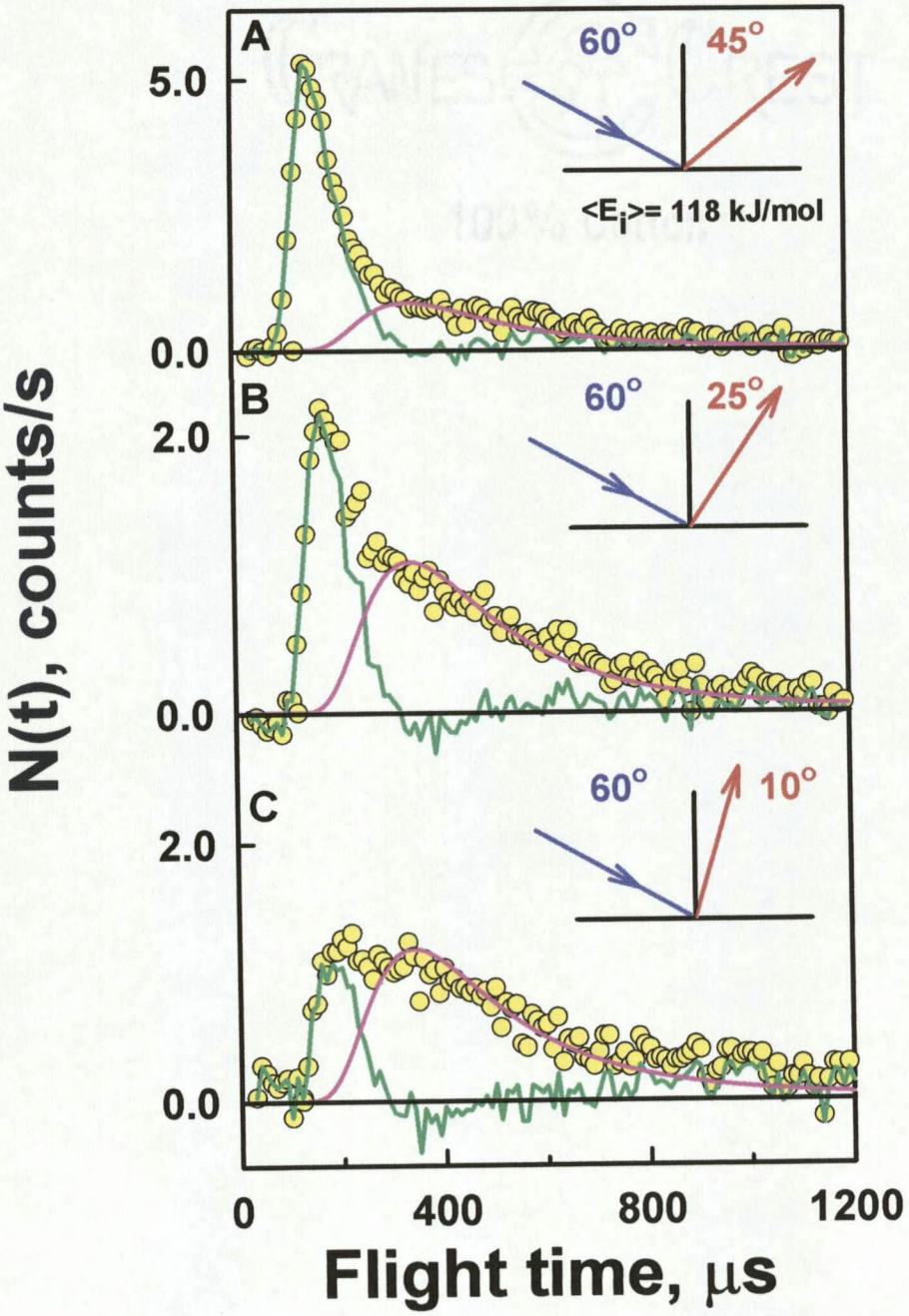

Figure 3-10. Representative time-of-flight distributions for scattered Cl following impact with the squalane surface. The chlorine beam had an energy of 118 kJ/mol and the was incident to the surface at 60° and the scattered Cl was detected at three final angles, 45°, 25°, and 10°.

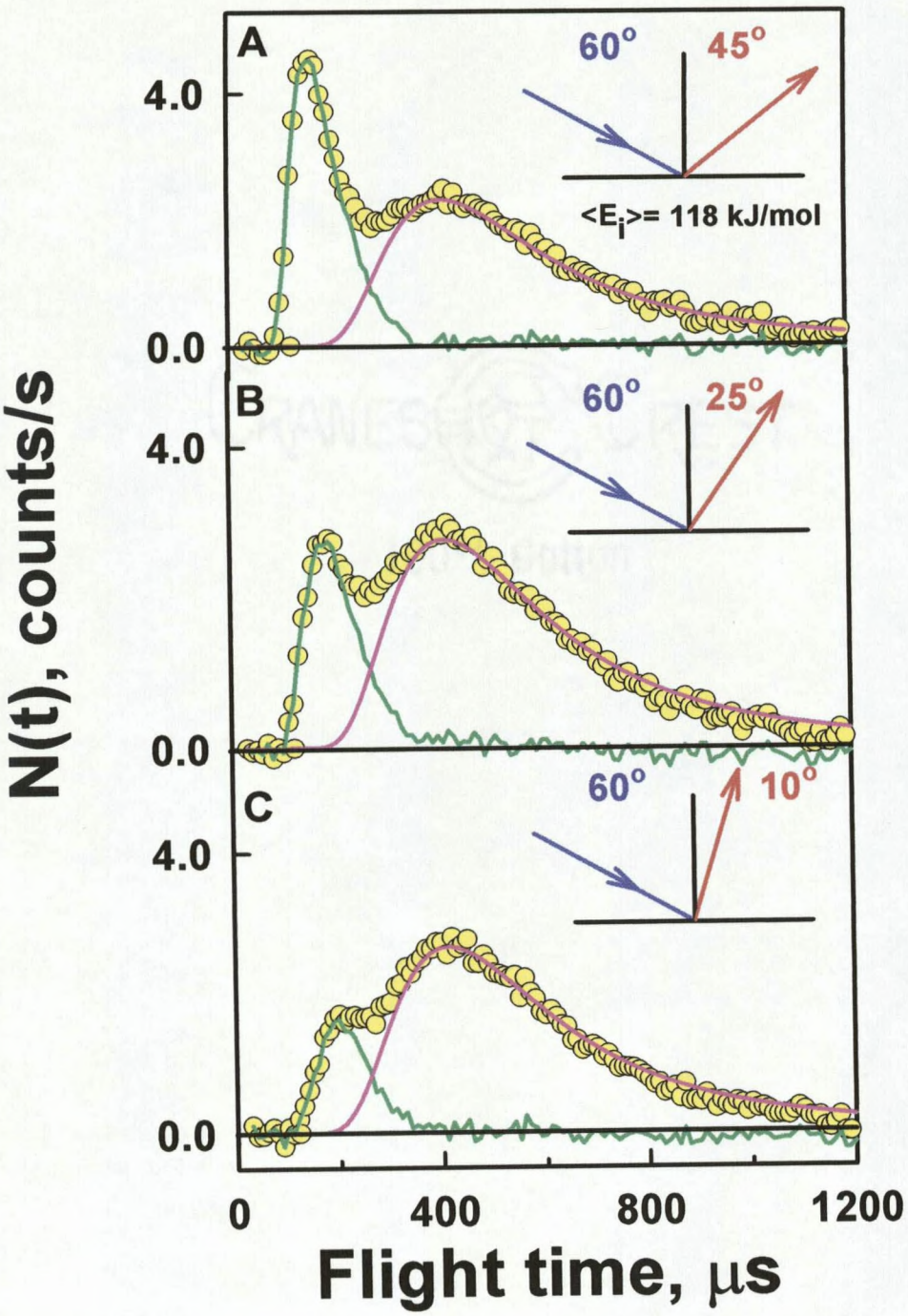

Figure 3-11. Representative time-of-flight distributions for reactively scattered HCl following reaction of an 118 kJ/mol incident chlorine atom beam with the squalane surface. The incident angle of the beam was 60° and three detected angles, 45°, 25°,and 10° are shown.

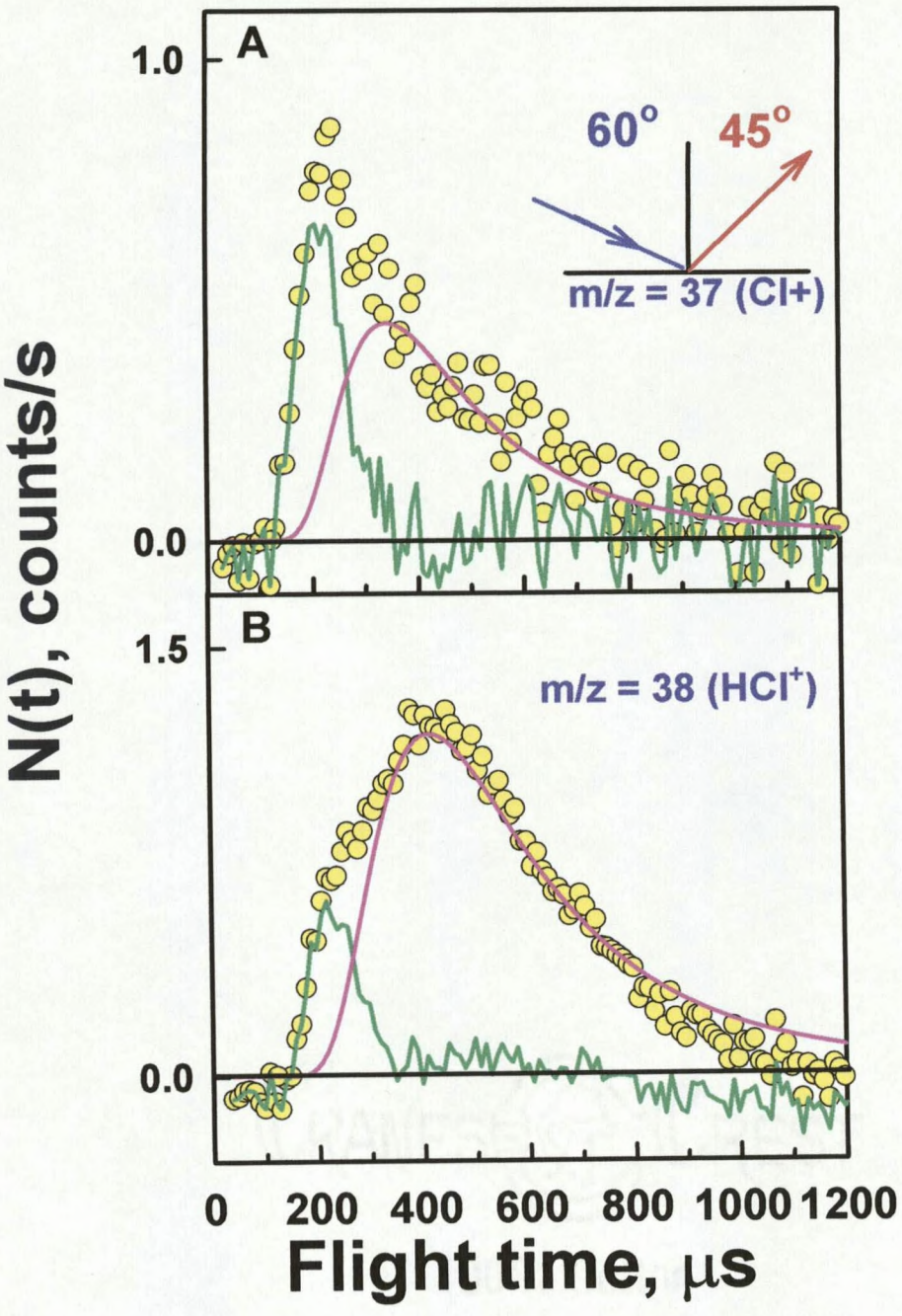

Figure 3-12. Representative time-of-flight distributions for Cl (top) and HCl (bottom) following interaction of 43 kJ/mol chlorine atoms with the squalane surface. The chlorine beam had an incident angle of 60° and only one detected angle, 45°, is shown.

hyperthermal Cl approaches zero at the maximum available energy (the maximum in the incident beam energy distribution) for the most "glancing" collision observed ($\theta_i = 60°$ and $\theta_f = 45°$). The amount of energy transfer increased as the detected angles became less glancing. The HCl reactive product exhibited the same behavior. However, the average final energies of the hyperthermal HCl component were less than those of the hyperthermal Cl component. Still, the translational energy distribution for HCl also approached zero at the maximum translational energy of the incident beam for an incident angle of 60° and a final angle of 45°. The abstraction of a hydrogen atom is expected to have essentially no barrier (a few kJ mol^{-1}) and to be slightly exothermic ($-\Delta H \cong$ 2-30 kJ mol^{-1}, depending on the type of hydrogen abstracted). Adding the exothermicity to the maximum translational energy of the incident beam yields the maximum available energy, $E_{avl}(max)$. The HCl exits the surface with translational energies that are lower than $E_{avl}(max)$.

Fig. 3-15 shows the fractional energy transfer of Cl and HCl and O and OH with the surface as a function of deflection angle, defined as $180° - (\theta_i + \theta_f)$. The shapes of both curves are very similar but do not follow the single-collision hard sphere model of interaction.

The angular distributions of the two components of scattered Cl and HCl flux for $\theta_i = 60°$ and $\langle E_i \rangle = 118$ kJ mol^{-1} are shown in Fig. 3-16. The thermal components follow a cosine distribution, as expected, and the hyperthermal components are much narrower than a cosine distribution and have maxima far from the surface normal (47° in the case of HCl).

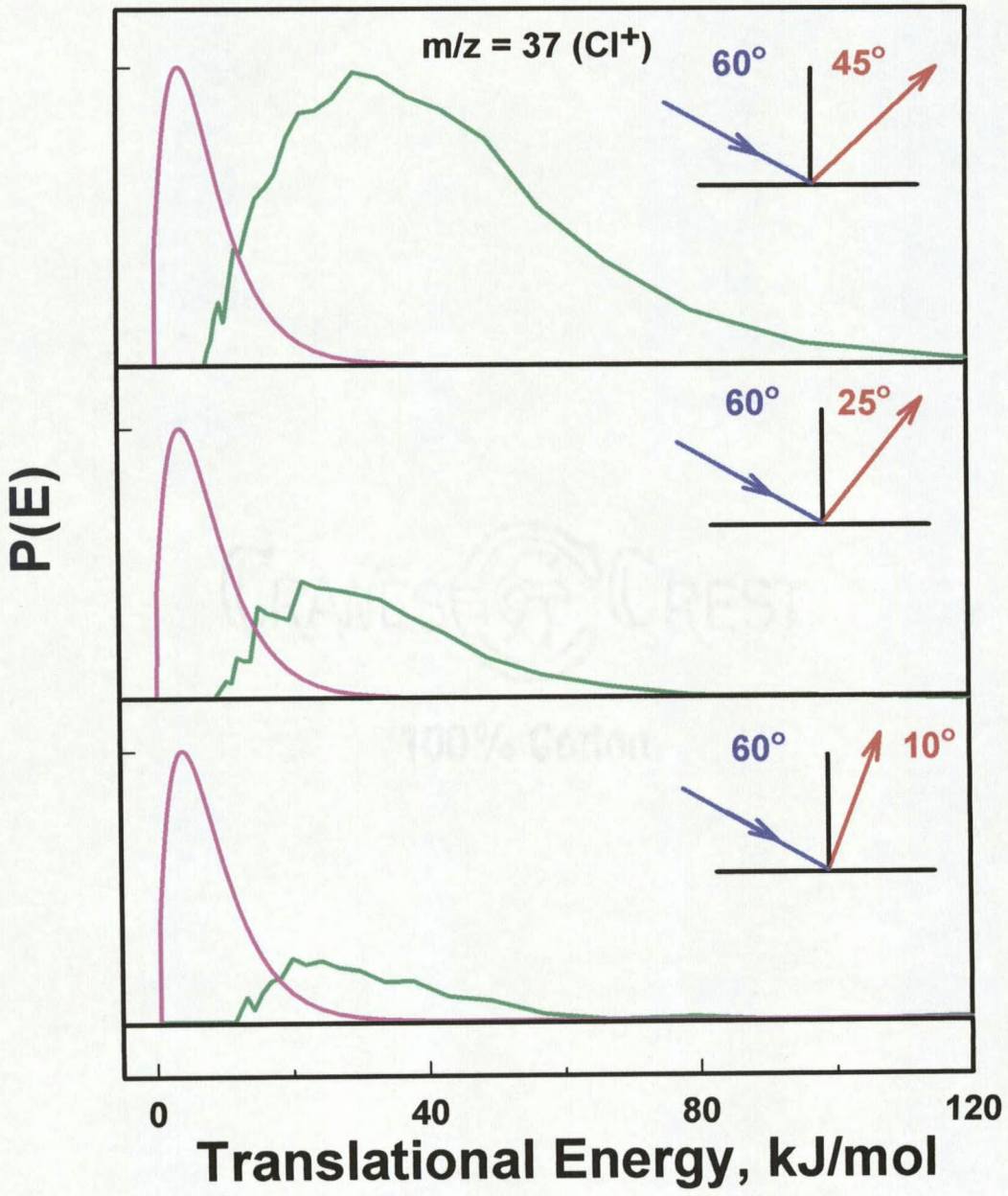

Figure 3-13. Translational energy distributions of scattered Cl derived from the time-of-flight distributions shown in Fig. 3-10. All detected angles contained a hyperthermal (green) and thermal (pink) component.

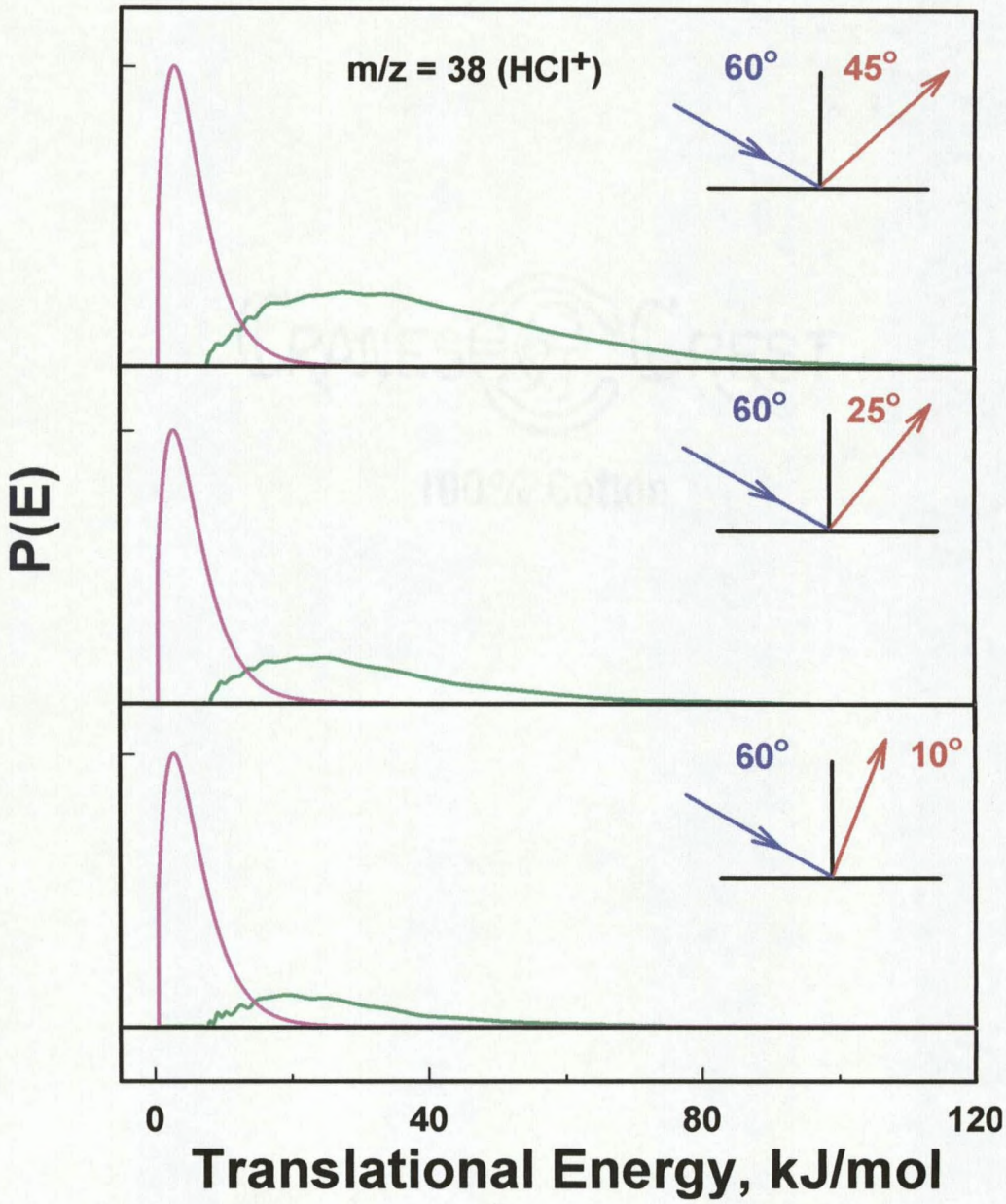

Figure 3-14. Translational energy distributions of reactively scattered HCl product derived from the time-of-flight distribution shown in Fig. 3-11. All detected angles contained a hyperthermal (green) and thermal (pink) component

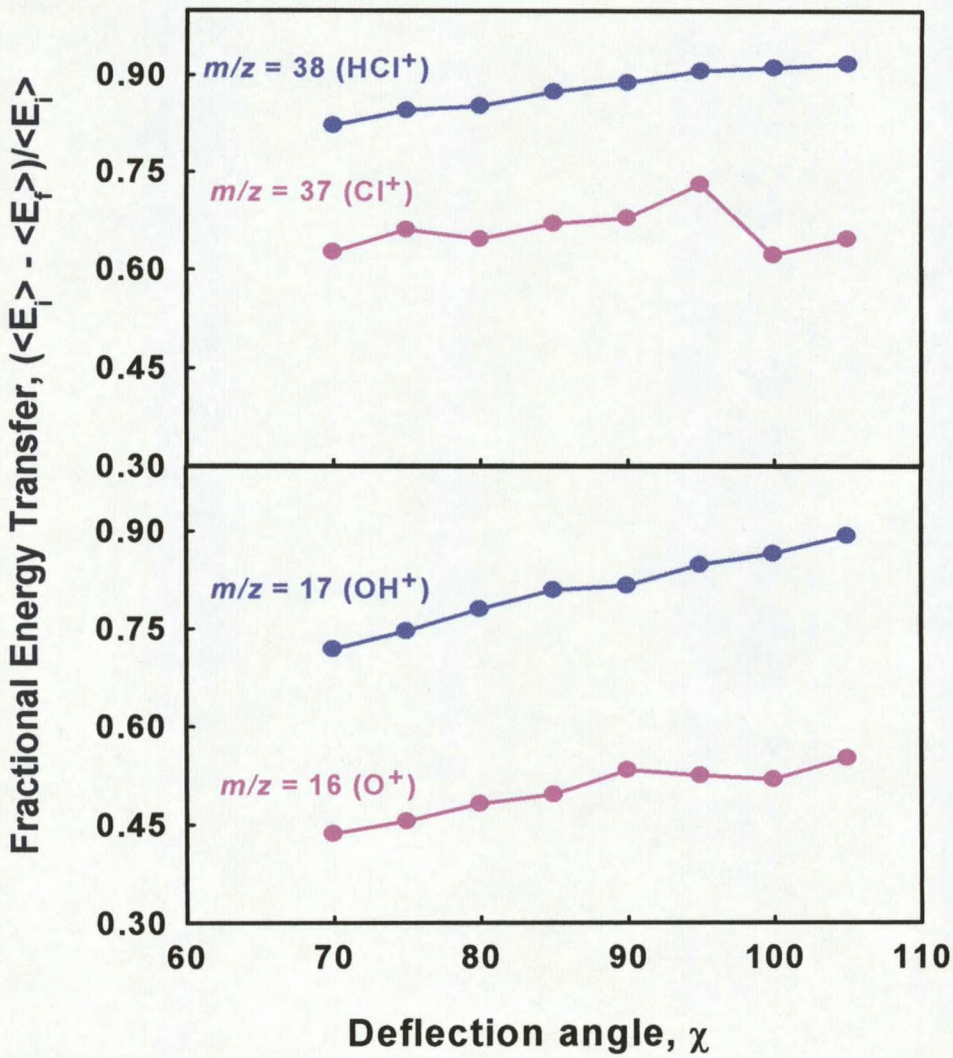

Figure 3-15. **A.** Fractional energy transfer of hyperthermal Cl and HCl as a function of deflection angle for $\theta_i = 60$ and $\langle E_i \rangle = 118$ kJ/mol.
B. Fractional energy transfer of hyperthermal O and OH as a function of deflection angle for $\theta_i = 60$ and $\langle E_i \rangle = 47$ kJ/mol.

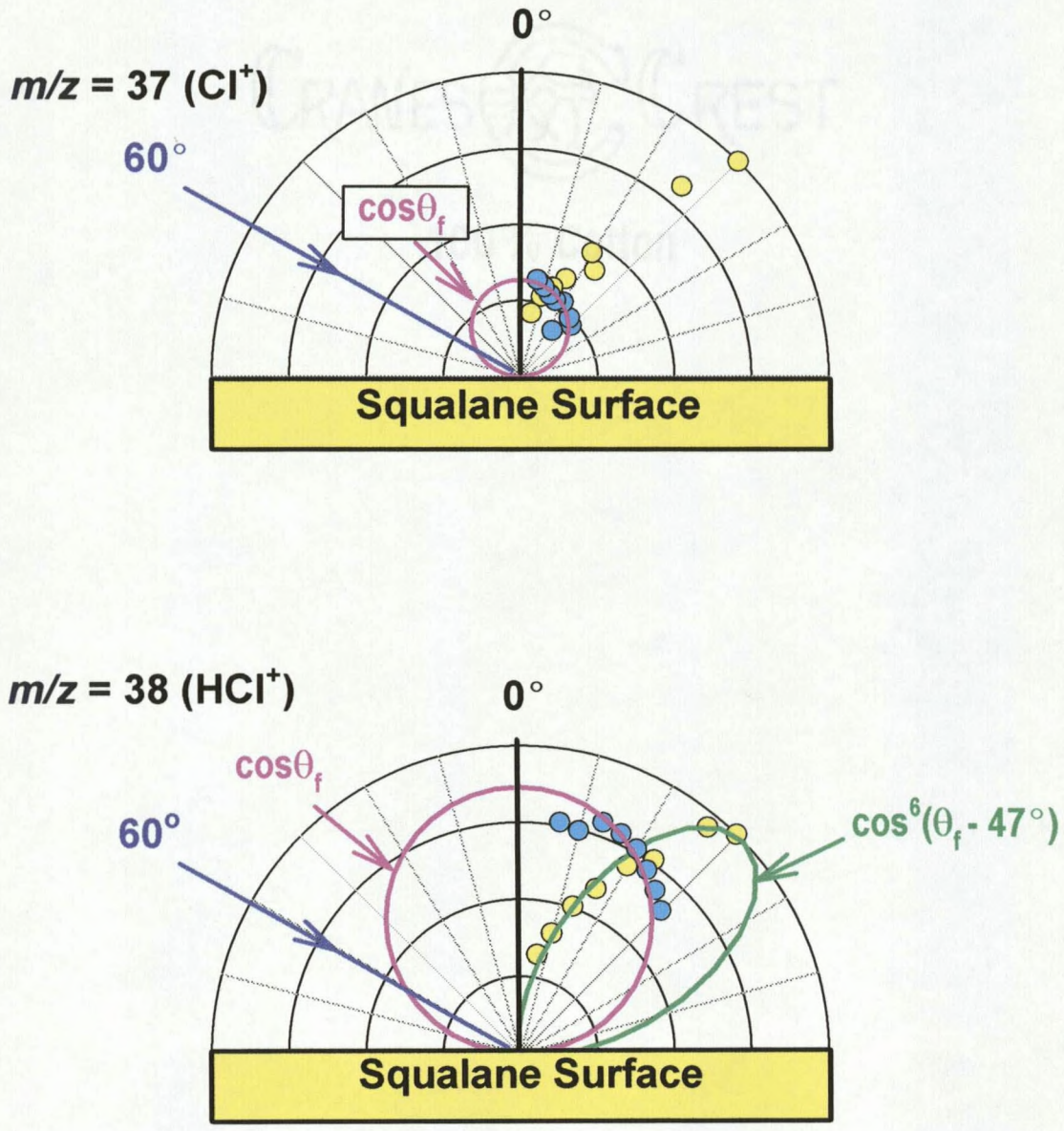

Figure 3-16. Angular distribution of Cl and HCl flux following Cl-atom impact with squalane at $\langle E_i \rangle$ = 118 kJ/mol and θ_i = 60. The thermal components follow a cosine distribution. The hyperthermal components are peaked away from the surface normal and are narrower than cosine.

CHAPTER 4

QUALITATIVE DESCRIPTION OF O-ATOM REACTIONS

Initial Reactions

The dynamical properties of the hyperthermal OH product indicate that it is formed through a direct abstraction (Eley-Rideal) mechanism. Rettner and Auerbach have pointed out that direct atom-surface reactions yield products with hyperthermal translational energies that are proportional to incident energy and with angular distributions that are asymmetric with respect to the surface normal.[52] The hyperthermal H_2O signal cannot correspond to a single-collision mechanism. The sum of two direct reactions, initial formation of OH and subsequent abstraction of another H atom, is the simplest explanation for the nonthermal H_2O products.

TOF distributions of O, OH, and H_2O exhibit substantial slow components. The shape of these slow components may be described very well by assuming a Maxwell-Boltzmann distribution of translational energies. The slow flux at all three detected masses follows a $\cos\theta_f$ functional form. These observations indicate that the slow components in the TOF distributions correspond to mechanisms whereby the incident atom or reactive product reaches thermal equilibrium at the surface before desorbing.

The atomic oxygen beam contains $O(^3P)$ and $O(^1D)$, both of which may react at the hydrocarbon surface. Kinetic studies of gas-phase reactions of atomic oxygen with saturated hydrocarbons at room temperature have shown that rate constants for $O(^1D)$ reactions are near gas kinetic and can be as much as 4 orders of magnitude greater than those for $O(^3P)$ reactions. However, at higher temperatures (~2000 K) rate constants for $O(^3P)$ reactions increase dramatically and may reach values close to half the $O(^1D)$ reaction rate constants.[53] Although the incident O-atom energy distributions are not Maxwellian, the high average energies of 21 and 47 kJ mol^{-1} make comparison with high temperature rate data most relevant. Based on an estimated $O(^1D)/O(^3P)$ ratio in the beam of 0.05, we might therefore expect that the fraction of reactions at the surface that involve $O(^1D)$ is in the range of 10 - 20 percent.

The experimental data suggest that the volatile reaction products come almost entirely from $O(^3P)$ reactions at the surface. The only products observed were OH and H_2O. There was no evidence for a product, such as CH_2OH, that would be unique to an $O(^1D)$ insertion reaction. Figure 3-9 shows that the TOF distributions of the OH product are essentially identical when the $O(^1D)/O(^3P)$ ratio is reduced by about 40 percent. Furthermore, the translational energy distributions of the OH products from the reaction with the higher-energy beam appear to go to zero near the maximum available energy for an $O(^3P)$ reaction. (Note that reactions with $O(^1D)$ would have an additional 189.8 kJ/mol of energy available for translation.) With the lower-energy beam, the translational energy distribution (Fig. 3-6B) revealed a small energetic tail at energies higher than possible if the only reactions involved $O(^3P)$; however, this tail accounts for <5 percent of the scattered flux.

The minimal experimental evidence for any distinct $O(^1D)$ reactive channel can be largely attributed to the expected chemical behavior of $O(^1D)$. In gas-phase reactions, $O(^1D)$ reacts with hydrocarbons primarily (perhaps exclusively) by insertion into a C–H bond, which leads to an excited alcohol intermediate. For gaseous hydrocarbon reactants larger than CH_4, the excited alcohol dissociates almost entirely via cleavage of a relatively weak C–C bond with greater than 90 percent probability.[23] The activated complex may be stabilized if the pressure is high enough to allow collisional quenching before dissociation occurs, although some OH product signal is observed even at high pressures.[20] Naaman and coworkers also found a minor channel in the reaction of $O(^1D)$ with propane clusters that leads to the prompt formation of OH, presumably because $O(^1D)$ crosses to a triplet surface and reacts adiabatically.[25] Complete stabilization of the hot alcohol in reactions of $O(^1D)$ with ethane and propane dissolved in liquid argon was reported.[53] If $O(^1D)$ inserts into a C–H bond on the liquid surface, then it is likely that the activated complex would be stabilized, leaving an alcohol intact. The lack of observation of an insertion product signal (e.g, CH_2OH) supports the conclusion that the alcohol intermediate is indeed stabilized at the surface. Any volatile products of $O(^1D)$ reactions would result from a minor competing direct mechanism, as has been observed in gas-phase reactions. Evidence of this direct mechanism was observed only in the experiment with the lower-energy beam. When the incident energy is decreased, the $O(^3P)$ reaction cross section would be expected to decrease significantly relative to the $O(^1D)$ cross section. In addition, the reduced incident energy would lead to an increased probability for the singlet-triplet crossing. Therefore, the contribution of $O(^1D)$ to the reactive signal should be more discernable when the incident

energy is lowered.

Given the facts that the atomic component of the beam strongly favors $O(^3P)$, which can only react by an abstraction mechanism, and that the $O(^1D)$ atoms in the beam are unlikely to form OH by a direct mechanism, we conclude that the volatile products which we observe must arise from ground-state $O(^3P)$ reactions. This explanation is consistent with the identical TOF distributions collected for OH even when the $O(^1D)$ fraction in the beam was reduced by 40 percent and with the translational energy distributions that fall to zero near the maximum energy available for $O(^3P)$ reactions. The long, albeit small, energetic tail on the OH translational energy distributions corresponding to reactions with the lower-energy beam may be attributed to the relatively few direct reactions involving $O(^1D)$. With the exception of this high-energy tail in the OH translational energy distributions, we have seen no distinct evidence for $O(^1D)$ reactions. The data are consistent with the gas-phase observation that insertion reactions dominate and lead to activated complexes that may be stabilized before dissociation. If direct reactions involving $O(^1D)$ occur to any appreciable extent, then the OH translational energy distributions for both these reactions and $O(^3P)$ abstraction reactions (for a given incident energy) must be similar.

While comparisons with gas-phase reactions are helpful in explaining the lack of a distinct $O(^1D)$ signal, the thermal products must be the result of unique surface processes. The TOF distributions of inelastically scattered O atoms show both hyperthermal and thermal components, which may be described by two limiting cases of inelastic scattering and trapping desorption, respectively.[54] The existence of a trapping desorption component implies that atomic oxygen can be trapped on the surface long enough to reach thermal

equilibrium. It is possible that thermalized $O(^3P)$ atoms may react with the hydrocarbon surface through a mechanism that involves triplet-singlet crossing of a long-lived collision complex. Naaman and coworkers[26] have reported that the reaction of thermal $O(^3P)$ with cyclohexane clusters leads to bond insertion on a singlet surface and subsequent alcohol formation. While such reactions may indeed be occurring, they are not expected to yield volatile OH products, as the alcohol should be stabilized on the surface. The more likely explanation for thermal OH is that direct abstraction is followed by thermal accommodation of the OH product on the surface. Once OH becomes thermally accommodated on the surface, it may desorb thermally or abstract another hydrogen atom to form H_2O,[55] which could also desorb thermally.

The fraction of thermal desorption in the OH signal increases when the incident beam energy is reduced. The TOF distributions of the unreactive O atoms parallel this behavior. Whether incident O atoms or product OH radicals impinge on the surface, the trapping probability increases with decreasing incident energy. Thus, the thermal component is larger relative to the hyperthermal component in the TOF distributions when the average beam energy is lower.

The dynamical information that we have been able to infer from our scattering data have led to a qualitative picture (Fig. 4-1) of the initial interactions between hyperthermal oxygen atoms and a hydrocarbon surface. The balance between the various possible reaction pathways is certainly dependent on incident energy and incident and final angles. Note especially that the relative importance of the nonthermal processes increases dramatically at high incident energies.

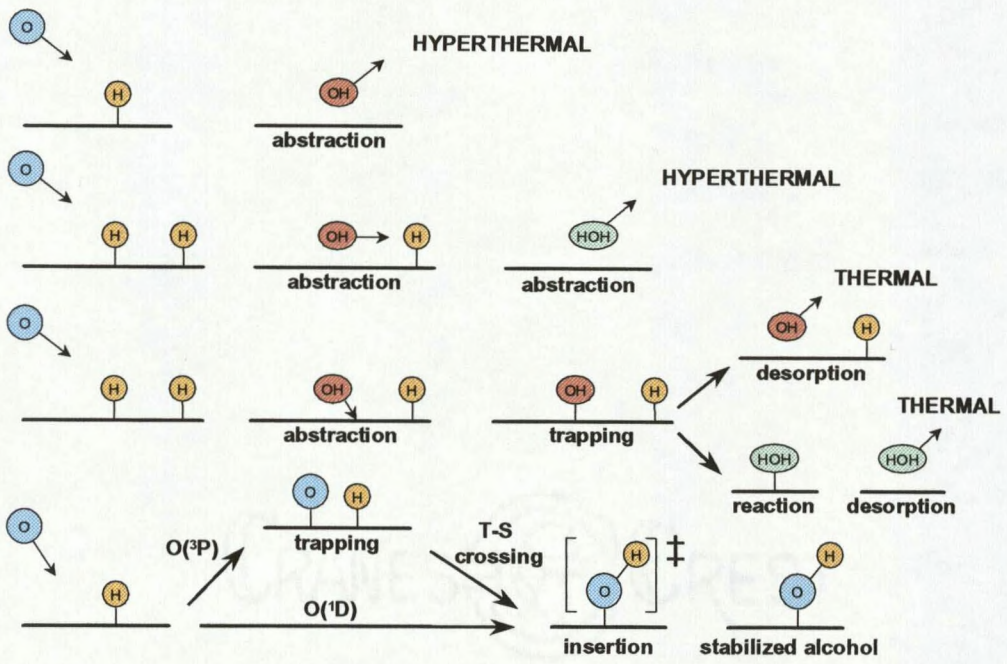

Figure 4-1. Summary of the initial reaction mechanisms inferred from the experiment with the liquid squalane surface.

In conclusion, the dynamics of initial oxygen-atom reactions at a saturated hydrocarbon surface were studied by directing an O-atom beam at a continuously-refreshed liquid squalane surface and monitoring energy and angular distributions of the volatile reaction products. Two beams were used, with average O-atom translational energies of 21 and 47 kJ mol^{-1}. Both beams contained ground-state $O(^3P)$ and electronically excited $O(^1D)$ with similar mixing ratios of approximately 1.00:0.05. The major reaction product, OH, was formed in two populations, which were characterized by their translational energy distributions as hyperthermal or thermal. The dynamical behavior of the hyperthermal OH signal clearly identified it as the result of a direct mechanism, predominantly H-atom

abstraction. The mechanism for production of thermal OH probably involves a sequential process whereby the initial OH abstraction product becomes thermally accommodated on the surface and then desorbs. This process is somewhat analogous to trapping desorption in gas-surface inelastic scattering. The only other reaction product observed was H_2O, which also exited the surface with hyperthermal and thermal populations, although the thermal H_2O products were overwhelmingly dominant. The most plausible mechanism for the formation of hyperthermal H_2O is direct abstraction of an H atom by the initial hyperthermal OH product. Apparently, a much more probable route to H_2O is a thermal reaction between trapped OH and the hydrocarbon chain. It is unlikely that oxygen atoms which thermally accommodate on the surface can lead to volatile reaction products. Thermal $O(^3P)$ will react with a saturated hydrocarbon almost solely through a singlet-triplet crossing mechanism, in which case the O atom would insert into a C–H bond to yield an alcohol that would be stabilized in the liquid. $O(^1D)$ reactions are also expected to form stabilized insertion products with greater than 90 percent probability. We see no evidence for a volatile product of an $O(^1D)$ reaction, except for a small OH signal that is too energetic to come from an $O(^3P)$ reaction. This signal is most likely the result of a relatively improbable $O(^1D)$ direct reaction. In summary, all data are consistent with the conclusion that the first step toward volatile reaction products, whether thermal or hyperthermal, is a direct reaction to form OH.

Loss of Carbon from Polypropylene under Steady-State Bombardment by O Atoms

The large signals observed at m/z = 28 and 44 for polypropylene as compared with squalane imply that complete oxidation of the hydrocarbon and subsequent desorption of stable CO and CO_2 products occur under continuous O-atom bombardment. The bimodal TOF distributions (fig 3-4) indicate thermal and nonthermal mechanisms. The mechanisms are undoubtedly complex. Oxides may form on the surface through insertion reactions. Furthermore, once a radical site is formed, it will be susceptible to subsequent O-atom reactions. We have seen that reaction sequences ultimately lead to the formation of the end products of combustion, CO and CO_2. These products may either desorb from the surface spontaneously or be ejected via a direct collisional event, such as collision-induced desorption or direct reaction.

CHAPTER 5

COMPARATIVE DYNAMICS OF Cl(^2P) AND O(^3P) REACTIONS

The dynamical behavior of the HCl product was analogous to the OH product. The bimodal TOF distributions indicated two general reactive processes at the surface, one thermal and the other nonthermal. The nonthermal process led to hyperthermal products that were assigned, in the case of OH, to a direct abstraction Eley-Rideal mechanism. The hyperthermal HCl products meet the same criteria for assignment as an Eley-Rideal mechanism: the average final energies of the HCl products are hyperthermal and are proportional to the incident beam energy and their angular distributions are not cosine, with maximum scattered flux displaced from the surface normal. Whether an O atom or a Cl atom encounters a hydrocarbon surface, it appears that a major reaction pathway is H-atom abstraction that is reminiscent of gas-phase reactions of these atoms with alkanes.

The dynamics of the gas-phase hydrogen-abstraction reactions are typically studied by observing the scattering directions (in the center-of-mass frame) and either internal state distributions or translational energy distributions of the OH and HCl products. Our experiments do not provide information on internal states, but we can examine the variation of product flux and translational energy with angle in order to gain insight into the nature of the reaction at the surface. A major difference between our data and gas-phase dynamical

data is that the products appear to scatter preferentially in the forward direction, as seen in Figs. 3-8 and 3-15. If the surface is rough enough such that an incident atom scatters off a protruding group in much the same way as it would scatter from an isolated molecule, then we would expect to see a substantial backward-scattered component. It has been inferred that there is a strong preference for the collinear O–H–C geometry in the transition state of the reaction of an O atom with an alkane, implying small impact parameter collisions and backward scattering of the OH product.[14-16] This is also true for the atomic chlorine reactions, but with a less restrictive collinear requirement. If the observed angular distributions were extrapolated according to the fitting functions shown in Figs. 3-8 and 3-15, then we would infer that very little OH or HCl would be backward scattered at angles in the vicinity of the reverse direction of the incident beam. The apparent absence of backward scattering might lead to the conclusion that the surface is smooth and that the resulting dynamics could be viewed as a heavy incident atom being approximately specularly scattered, having stripped an H atom from the flat surface.

Many studies indicate that the surface of squalane is rough on an atomic scale. Inelastic scattering experiments of rare gas atoms on squalane show that energy transfer depends on the angle of deflection, indicating that the incident atoms undergo hard sphere-like collisions at the surface.[56] Theoretical modeling studies of similar organic liquid surfaces reveal rough surfaces that are dominated by hydrocarbon chain ends.[44] In our experiments, the translational energies of the hyperthermal O, OH, Cl, and HCl products increased with final angle for grazing incidence collisions, again indicative of scattering from a highly-corrugated surface.

Even though the surface is rough, the OH and HCl products might not necessarily scatter predominantly into the direction of the incoming beam. Such backward scattering would occur if the carbon atom to which the reacting H atom is attached had an infinite effective mass as a result of being tethered to the surface and if the reaction occurred via a collinear attack by the O atom on the C–H bond. Given these constraints, the product would have to carry away all the available energy. In fact, these constraints are considerably more relaxed. If we assume that an incoming O or Cl atom undergoes a single, gas-phase-like H-atom abstraction reaction with a local fragment of a squalane molecule at the surface, then we can construct a Newton diagram from our data that gives the effective mass of the collision partner at the surface. Figs. 5-1 and 5-2 show such Newton diagrams for HCl and OH, respectively, for an incident angle of 60°, with the higher-energy incident atoms. The product velocity at each final angle was derived from the average final energy of the hyperthermal signal at that angle. If the final velocity is fairly constant as a function of the center-of-mass (c.m.) scattering angle, then the product velocities in this velocity vector diagram should lie on a circle about the c.m. It does appear that the product velocities lie on a circle about a point on the relative velocity vector, which is where the c.m. must be. If we take this point as the c.m., then we can calculate the velocity of the c.m., the c.m. velocities of the two collision partners, and the effective mass of the part of the surface that is reacting; these values are shown in the figures. The effective surface mass for the O-atom reaction is 83 amu, while that for the Cl-atom reaction is 230. In the c.m. frame given by these Newton diagrams, the product flux seems to be sideways and even somewhat

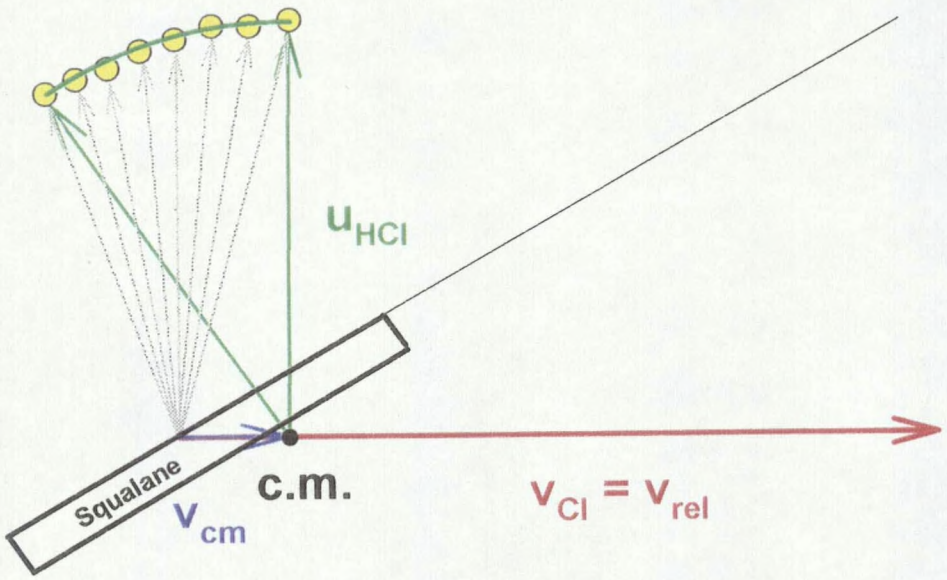

Figure 5-1. A Newton diagram for the interaction of 118 kJ/mol Cl atoms with a squalane surface. The chlorine beam is incident at 60°. By assuming the reaction occurred in a single bounce and the velocity of the exiting HCl product is constant, the interaction can be converted into the center of mass frame. The effective mass of the surface can then be calculated using

$$m_S = m_{Cl}\left(\frac{v_{Cl}}{v_{cm}} - 1\right) = 230 \text{ amu} \quad . \qquad (1)$$

Once the effective surface mass is known, the collision energy and center-of-mass energy can then be determined by using the following equations:

$$E_{coll} = \frac{1}{2}\mu\, v_{rel}^{2} = 102 \text{ kJ mol}^{-1} \qquad (2)$$

$$E_T = \frac{1}{2} m_{HCl} u_{HCl}^{2} + \frac{1}{2} m_S u_S'^{2} = 276 \text{ kJ mol}^{-1} \qquad (3)$$

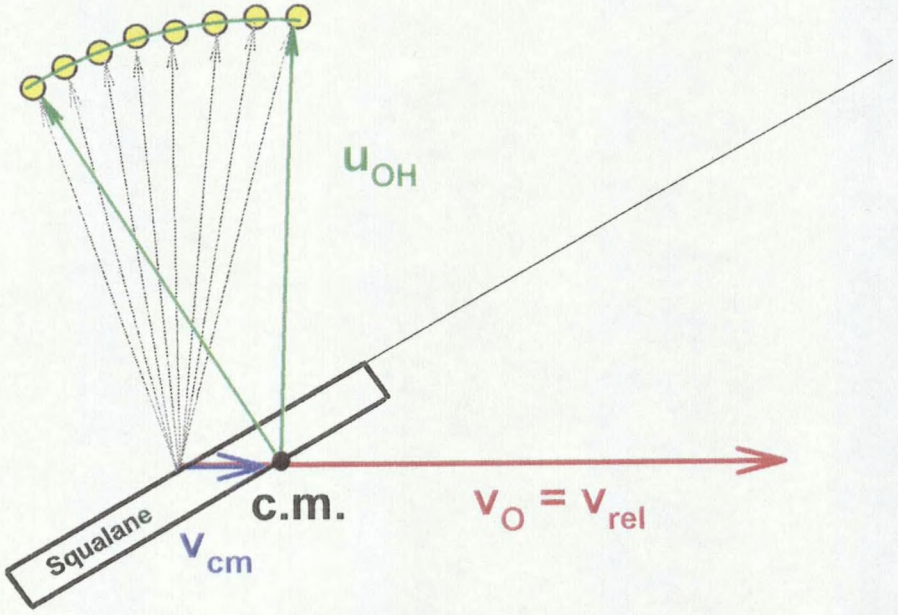

Figure 5-2. A Newton diagram for the interaction of 47 kJ/mol O atoms with a squalane surface. The incident angle is 60°. The effective surface mass was calculated using equation (1) to be 83 amu. From equations (2) and (3) the collision energy and total center-of-mass energy were determined to be 39.4 and 39 kJ/mol, respectively.

backward scattered. The surface, though rough, still constrains the range of impact parameters at a given point. Thus collinear geometries that dominate gas phase reactions might be unfavorable, and lower-cross-section but more-probable off-axis geometries could dominate the gas-surface abstraction reactions, giving rise to diffuse scattering that has a propensity for the sideways direction. As discussed in the Introduction, the gas-phase reactions are not necessarily constrained to a collinear geometry. The related reactions of

Cl + alkanes show significant sideways scattering of the propyl (and therefore HCl) product in the angular distributions. Such distributions are lacking in the studies of $O(^3P)$ + gas-phase saturated hydrocarbons. Given the similarity of the scattering behavior of the atomic chlorine and oxygen reactions with squalane in our experiments, we might conclude that the gas-phase dynamics of O-atom reactions with alkanes would resemble those of the analogous Cl-atom reactions, with a relaxed constraint on the collinear transition state geometry.

The range of final angles in our experiments is limited, and the $\cos^n\theta_f$ distribution was only used to show that the product angular distribution was much narrower than cosine. This chosen "fitting function" has no particular physical significance. It is possible that the angular distribution is more complicated than our data imply. There might even be an enhancement at negative final angles that were inaccessible in our experiment.

The thermal HCl product may be formed by trapping of the initial HCl abstraction product on the surface (analogous to the mechanism that was inferred for the production of thermal OH), or it may be formed by a reaction that takes place in thermal equilibrium with the surface after the incident chlorine atom becomes trapped. This second mechanism is possible because of the low barrier to reaction. Kinetic data suggest that Cl will abstract an H atom from a hydrocarbon molecule even at 300 K.[29] In the reaction of $O(^3P)$ with squalane, the barrier is on the order of 20 kJ mol^{-1}, so available energy is not sufficient for the O atom to react at 300 K.

Examination of the relative behavior of the thermal component in the inelastic and reactive signals provides evidence for a mechanism in which thermalized chlorine atoms can react on the surface. The data from the O + squalane experiment showed equal fractions of

the thermal component (0.3) in the translational energy distributions of O and OH for $\theta_i = \theta_f = 45°$ and $\langle E_i \rangle = 47$ kJ mol^{-1}. The fractions of the thermal components in the Cl and HCl translational energy distributions (for $\theta_i = \theta_f = 45°$ and $\langle E_i \rangle = 43$ kJ mol^{-1}) were 0.7 and 0.8, respectively. This increase in the reactive thermal fraction relative to the inelastic thermal fraction in the Cl-atom experiment as compared to the O-atom experiment suggests that trapped chlorine atoms are reacting. When trapped Cl atoms react, the thermal component of the inelastic signal is reduced while the thermal component of the reactive signal is enhanced. Unfortunately, our data only allow us to confirm that trapped Cl atoms can react to produce volatile HCl; we are not able to identify the relative fractions of HCl products that come from reactions of trapped Cl atoms versus those that come from trapping of HCl that is produced directly.

The hyperthermal and thermal HCl and OH products from the reaction of Cl and O atoms from the squalane surface seem to exhibit very similar dynamics. In both reactions, the hyperthermal products are formed through a direct abstraction, E-R mechanism. These products appeared forward-scattered in the lab frame which would imply a light interaction of the incident atoms with hydrogen atoms a smooth surface. Further investigation reveals that when the systems are converted into the center of mass frame, the scattering is sideways and backwards scattered, consistent with a rough squalane surface and observed gas phase behavior. The effective surface mass for the squalane surface was about a half the mass of a squalane molecule for the Cl atom interaction and a quarter for the O atom interaction. The thermal signal for the atomic oxygen reaction with squalane arises solely from trapping and subsequent desorption of OH product formed by direct reaction. This trapping and

desorption is most likely contributing to the thermal HCl signal along with a thermal reaction mechanism possible in the Cl atom reactions.

REFERENCES CITED

1. C. T. Rettner and D. J. Auerbach, *Phys. Rev. Lett.*, **74** (1995) 4551.

2. W. H. Weinberg, *Acc. Chem. Res.*, **29** (1996) 479.

3. C. T. Rettner, *J. Chem. Phys.*, **101** (1994) 1529.

4. M. Xi and B. Bent, *J. Phys. Chem.*, **97** (1993) 4167.

5. C. Lutterloh, A. Schenk, J. Biener, B. Winter, and J. Küppers, *Surf. Sci.*, **316** (1994) L1039.

6. E. W. Kuipers, A. Vardi, A. Danon, and A. Amirav, *Phys. Rev. Lett.*, **66** (1991) 116.

7. F. D. Egitto and L. J. Matienzo, *IBM J. Res. Develop.*, **38** (1994) 423; E. M. Liston, *J. Adhes.*, **30** (1989) 199.

8. M. A. Hartney, D. W. Hess and D. S. Soane, *J. Vac. Sci. Technol. B.*, **7** (1989) 1.

9. O. Joubert, J. Pellitier and Y. Arnal, *J. Appl. Phys.*, **65** (1989) 5096; G. S. Selwyn, *J. Appl. Phys.*, **60** (1986) 2771.

10. C. M. Chan, T. M. Ko and H Hiroka, *Surf. Sci. Rep.*, **24** (1996) 1; A. S. Hoffman, *J. Appl. Polym. Sci. Appl. Polym. Symp.*, **42** (1988) 251.

11. L. J. Leger, NASA TM-58246, 1982; L. J. Leger and J. T. Visentine, *Aerosp. Amer.*, **24** (1986) 32; L. E. Murr and W. H. Kinard, *Am. Sci.*, **81** (1993) 152.

12. T. K. Minton, JPL Publication 95-17, Pasedena, CA, 1995.

13. A. Miyoshi, K. Tsuchiya, N. Yamauchia and H. Matsui, *J. Phys. Chem.*, **98** (1994) 11452.

14. P. Andressen and A. C. Luntz, *J. Chem. Phys.*, **72** (1980) 5842.

15. N. J. Dutton, I. W. Fletcher and J. C. Whitehead, *Mol. Phys.*, **52** (1984) 475.

16. G. M. Sweeney, A. Watson and K. G. McKendrick, *J. Chem. Phys.*, **106** (1997) 9172.

17. P. Michaud, G. Paraskevopoulos and R. J. Cvetanović, *J. Phys. Chem.*, **78** (1974) 1457.

18. H. Yamazaki and R. J. Cvetanović, *J. Chem. Phys.*, **41** (1964) 3703.

19. G. Paraskevopoulos and R. J. Cvetanović, *J. Phys. Chem.*, **50** (1969) 590.

20. G. Paraskevopoulos and R. J. Cvetanović, *J. Phys. Chem.*, **52** (1970) 5821.

21. C.-L. Lin and W. B. DeMore, *J. Phys. Chem*, **77** (1973) 863; R. D. van Zee and J. C. Stephenson, *J. Chem. Phys.*, **102** (1995) 6946.

22. A. C. Luntz, *J. Chem. Phys.*, **73** (1980) 1143.

23. C. R. Park and J. R. Wiesenfeld, *J. Chem. Phys.*, **95** (1991) 8166.

24. M. Brouard and J. P. Simons in *Advanced Series in Physical Chemistry: Vol. 6, The Chemical Dynamics and Kinetics of Small Radicals*, ed. A. F. Wagner and K. Liu, World Scientific, Singapore, 1995, ch. 18.

25. Y. Rudlich, Y. Hurwitz, G. J. Frost, V. Vaida and R. Naaman, *J. Chem. Phys.*, **99** (1993) 4500.

26. Y. Rudlich, Y. Hurwitz, S. Lifson and R. Naaman, *J. Chem. Phys.*, **98** (1993) 2936.

27. P. Patiño, F. E. Hernández and S. Rondón, *Plasma Chem. Plasma Process.*, **15** (1995) 159.

28. S. P. Heneghan, P. A. Knoot and S. W. Benson, *Int. J. Chem. Kinet.*, **13** (1981) 677.

29. R. S. Lewis, S. P. Sander, S. Wagner and R. T. Watson, *J. Phys. Chem.*, **84** (1980) 2009.

30. A. Bottoni and G. Poggi, *J. Mol. Struct.*, **337** (1995) 161.

31. J. S. Pilgrim, A. McIlroy and C. A. Taatjes, *J. Phys. Chem. A.*, **101** (1997) 1873.

32. D. R. Lide, *Handbook of Chemistry and Physics, 76th ed*; CRC Press: Boca Raton, FL, 1995, chs. 5 and 9.

33. R. Atkinson, D. L. Baulch, R. A. Cox, R. F. Hampson, Jr., J. A. Kerr and J. Troe, *J. Phys. Chem. Ref. Data*, **21** (1992) 1125.

34. D. Varley and P. Dagdigian, *Chem. Phys. Lett.*, **255** (1996) 393.

35. W. R. Simpson, A. J. Orr-Ewing and R. N. Zare, *Chem. Phys. Lett.*, **212** (1993) 163.

36. W. R. Simpson, T. P. Rakitzis, S. A. Kandel, A. J. Orr-Ewing and R. N. Zare, *J. Chem. Phys.*, **103** (1995) 7313.

37. S. A. Kandel, T. P. Rakitzis, T. P. Lev-On and R. N. Zare, *J. Chem. Phys.*, **105** (1996) 7550.

38. W. R. Simpson, T. P. Rakitzis, S. A. Kandel, T. Lev-On and R. N. Zare, *J. Phys. Chem.*, **100** (1996) 7938.

39. A. J. Orr-Ewing, W. R. Simpson, T. P. Rakitzis, S. A. Kandel and R. N. Zare, *J. Chem. Phys.* **106** (1997) 5961.

40. D. F. Varley and P. J. Dagdigian, *J. Phys. Chem.*, **99** (1995) 9843.

41. D. F. Varley and P. J. Dagdigian, *J. Phys. Chem.*, **100** (1996) 4365.

42. Y. Yen, Z. Wang, B. Xue and B. Koplitz, *J. Phys. Chem.*, **98** (1994) 4.

43. D. Blank, Ph. D. Thesis, University of California, Berkeley, 1997.

44. J. G. Harris, *J. Phys. Chem.*, **96** (1992) 5077.

45. Y. T. Lee, J. D. McDonald, P. R. LeBreton and D. R. Herschbach, *Rev. Sci. Instrum.*, **40** (1969) 1402.

46. S. J. Sibener, R. J. Buss, C. Y. Ng and Y. T. Lee, *Rev. Sci. Instrum.*, **51** (1980) 167; P. Casavecchia, N. Balucani and G. G. Volpi, *in Advanced Series in Physical Chemistry: Vol. 6, The Chemical Dynamics and Kinetics of Small Radicals*, ed. A. F. Wagner and K. Liu, World Scientific, Singapore, 1995, p. 365.

47. K. Sköld, *Nucl. Instrum. Methods*, **63** (1968) 114.

48. M. Alagia, V. Aquilanti, D. Ascenzi, N. Balucani, D. Cappelletti, L. Cartechini, P. Casavecchia, F. Pirani, G. Sanchini and G. G. Volpi, *Isr. J. Chem.*, 1997, in press.

49. M. Alagia, N. Balucani, P. Casavecchia, D. Stranges and G. G. Volpi, *J. Chem. Soc.*

Faraday Trans., **91** (1995) 575.

50. M. E. Saeker, S. T. Govoni, D. V. Kowalski, M. E. King and G. M. Nathanson, *Science*, **252** (1991) 1421.

51. Signals detected at $m/z = 17$ contained a contribution from the ionizer fragmentation of H_2O products that was determined to be 21% of the signal detected at $m/z = 18$. Even when this contribution was subtracted from the $m/z = 17$ TOF distributions (as has been done in all data presented here), they clearly show two components.

52. J. T. Heron, *J. Chem. Ref. Data*, **17** (1988) 967.

53. W. B. DeMore, *J. Phys. Chem.*, **73** (1969) 391.

54. J. E. Hurst, C. A. Becker, J. P. Cowin, K. C. Janda, L. Wharton and D. J. Auerbach, *Phys. Rev. Lett.*, **43** (1979) 1175; C. T. Rettner, E. K. Schweizer and C. B. Mullins, *J. Chem. Phys.*, **90** (1989) 3800.

55. J. P. Abbatt, K. L. Demerjian and J. G. Anderson, *J. Phys. Chem.*, **94** (1990) 4566; R. Atkinson, *Chem. Rev.*, **86** (1986) 69.

56. M. E. King, G. M. Nathanson, M. A. Hanning-Lee and T. K. Minton, *Phys. Rev. Lett.*, **70** (1993) 1026.